5-1-2016

Strategic Molecular Design to Engineer the Electron Affinity of Self-Assembling Organic Semiconductors

Kelly Nicole Zaugg
University of Nevada, Las Vegas, zaugg@unlv.nevada.edu

STRATEGIC MOLECULAR DESIGN TO ENGINEER THE ELECTRON AFFINITY OF SELF-ASSEMBLING ORGANIC SEMICONDUCTORS

By

Kelly N. Zaugg

Bachelor of Science – Chemistry
University of Minnesota
2012

A thesis submitted in partial fulfillment
of the requirement for the

Master of Science – Chemistry

Department of Chemistry and Biochemistry
College of Sciences
The Graduate College

University of Nevada, Las Vegas
May 2016

UNLV | GRADUATE COLLEGE

Thesis Approval

The Graduate College
The University of Nevada, Las Vegas

April 5, 2016

This thesis prepared by

Kelly N. Zaugg

entitled

Strategic Molecular Design to Engineer the Electron Affinity of Self-Assembling Organic Semiconductors

is approved in partial fulfillment of the requirements for the degree of

Master of Science – Chemistry
Department of Chemistry and Biochemistry

Dong-Chan Lee, Ph.D.
Examination Committee Chair

Kathryn Hausbeck Korgan, Ph.D.
Graduate College Interim Dean

Gary Kleiger, Ph.D.
Examination Committee Member

Kathleen Robins, Ph.D.
Examination Committee Member

Woosoon Yim, Ph.D.
Graduate College Faculty Representative

ABSTRACT

Strategic Molecular Design to Engineer the Electron Affinity of Self-Assembling Organic Semiconductors

by

Kelly N. Zaugg

Dr. Dong-Chan Lee, Exam Committee Chair
Associate Professor of Chemistry
University of Nevada, Las Vegas

Development of electron-accepting (n-type) semiconductors used in organic photovoltaic cells and field effect transistors has been an area of research with less advancement compared to their electron-donating (p-type) counterparts. Currently, the highest performing n-type semiconductor is a fullerene-based derivative (PCBM) with a favorable E_{LUMO} of -4.08 eV. However, PCBM has limited absorption in the visible region and fixed electron affinity. This work focuses on the development of self-assembling n-type materials with controllable electronic properties by strategically lowering E_{LUMO} to a level comparable to PCBM. Molecular design follows an acceptor-acceptor'-acceptor (A-A'-A) configuration; with A being two 2,3-dioctyloxyphenazine substituents connected to A' with a C-C triple bond. A' was altered to increase the electron deficiency using benzothiadiazole (BTD), naphthalene diimide (NDI), and perylene-tetracarboxylic diimide (PTCDI). Based on this molecular design, four new n-type materials (**BTD-P**, **NDI-P-1**, **NDI-P-2**, **PTCDI-P**) were successfully synthesized with low E_{LUMO} values of -3.34 eV, -3.90 eV, -3.90, and -3.97 eV, respectively. Photophysical, thermal, and electrochemical properties were studied using UV-Visible absorption and fluorescence emission spectroscopy, differential scanning calorimetry, thermogravimetric analysis, and cyclic voltammetry. Theoretical evaluations were conducted to understand the experimental electronic

properties. Charge-transfer (CT) was also used to test the accepting properties of the title molecules when paired with a pyrene donor. Successful CT results were seen using **NDI-P-1**, which were confirmed through UV-Vis and fluorescence spectroscopy. The morphology of the CT complex was studied with polarized optical microscopy (POM). Additionally, fluorescence resonance energy transfer (FRET) through organogelation was studied with **BTD-P** as a donor with **NDI-P-2** as an acceptor. It was found that FRET was efficient even at low acceptor concentration of 5mole%. FRET results were characterized with fluorescence spectroscopy and POM.

ACKNOWLEDGEMENTS

I express my greatest gratitude towards my advisor, Dr. Dong-Chan Lee, who has guided me through the last two years giving me invaluable knowledge that helped me grow as a chemist. His constant insight paired with his broad intelligence has brightened my ambition and improved my diligence. I am extremely grateful to have such a supportive advisor that truly cares about my progress, even at times when I know I've managed to test his patience. He continues to push me towards greatness and has never accepted anything less.

I would also like to express gratitude towards my graduate committee members: Dr. Kathy Robins, Dr. Gary Kleiger, and Dr. Woosoon Yim. They have given me encouragement and provided helpful advice which has improved my thesis content. I appreciate their doors always being open and their willingness to help in any way they can. Their guidance has been of great importance for my academic advancement. Additionally, I'd also like to acknowledge partial financial support from National Science Foundation (DMR-0846479).

My gratitude continues to extend as I would also like to further thank UNLV Chemistry Department faculty including: Dr. Jun Young Kang, Dr. Pradip Bowmik, Dr. Haesook Han, for use of their chemicals and instruments; and Mark Miyamoto, Deborah Masters, and Carolyn Hatchett, for all of their assistance. I'd also like to give special thanks to my fellow students: Jungsoo Nam, Jung Jae Koh, John Velasco, Morgan Jarvis, Jason Sylva, Hayley Heers, and Samantha Itchon. These students have easily become good friends and have always been willing to help through many difficult times.

Outside the department, I have been extremely blessed with such a strong and supportive husband who has put up with my many complaints, late nights and stressful stages; but has always given me solid encouragement and stood by my side. My parents and in-laws also

deserve superior thanks for showing such praise and always believing in me. In addition to family, I couldn't have gotten through this without my amazing running friends. Being able to run off the stress and vent to friends has been a great way to stay focused. Without such great friends and family behind me, this accomplishment could never be possible.

TABLE OF CONTENTS

LIST OF TABLES

LIST OF FIGURES

LIST OF SCHEMES

LIST OF ABBREVIATIONS

HOMO	Highest Occupied Molecular Orbital
LUMO	Lowest Unoccupied Molecular Orbital
TCE	1,1,1-Trichloroethane
$CHCl_3$	Chloroform
$CDCl_3$	Deuterated Chloroform
CH_2Cl_3	Methylene Chloride
THF	Tetrahydrofuran
TEA	Triethylamine
NMR	Nuclear Magnetic Resonance
CV	Cyclic Voltammetry
FL	Fluorescence
1D	One Dimensional
3D	Three Dimensional
POM	Polarized Optical Microscopy
CT	Charge Transfer
FRET	Fluorescence Resonance Energy Transfer

1 INTRODUCTION

1.1 General Introduction

Development of electron-accepting (n-type) semiconductors used in organic photovoltaic cells and field effect transistors has been an area of research with less advancement compared to their electron-donating (p-type) counterparts.[1-4] In donor-acceptor organic solar cells or complimentary circuits, n-type is as important as it's p-type counterpart. Current examples of successful n-type design include fullerene (C_{60})[2,5] and its derivatives such as PCBM,[6-7] C_{70},[8-9] ICBA,[10] etc. All of which show high charge carrier mobility with three-dimensional (3D) charge transport, however their absorption is limited and electron affinity is fixed. Therefore, development of new n-type materials using non-fullerene based design with tailored electron affinity and light harvesting allows for advancement opportunities that address these limitations. However, creating new molecular design for n-type organic semiconductors that still combines high electron mobility with an appropriate LUMO energy level (E_{LUMO}) is challenging. One approach to maintaining efficient charge transport[1,11-12] has been observed in materials that have the ability to self-assemble into one-dimensional (1D) nanostructures.[13-16] Self-assembly can be achieved through intermolecular interactions such as π-π stacking and/or hydrogen bonding, making this a high priority in our molecular design. Additionally, we want materials with E_{LUMO} comparable to that of PCBM. Since PCBM is currently the highest performing n-type semiconductor with E_{LUMO} = -4.08 eV,[6] our molecule design should focus on achieving a comparable low lying E_{LUMO}. Typically, to be a useful n-type material for organic solar cell and field effect transistor, the electron-affinity should be in the range of 3.8-4.5 eV.[17-19] To accomplish this, it is logical to incorporate strong acceptors into the structure. Examples of structural moieties known for high electron withdrawing ability are benzothiadiazole (BTD),

naphthalene diimide (NDI) and perylene diimide (PTCDI), with E_{LUMO} levels of -2.87 eV,[20] -3.79 eV,[21] and -4.06 eV,[22-23] respectively. The design principle utilizing BTD, NDI, and PTCDI to create self-assembling n-type materials will be discussed in the next section.

When 1D self-assembling fibers with high electron affinity are successfully created based on our new molecular design strategy, the efficacy of their utility in charge transfer (CT) and fluorescence resonant energy transfer (FRET) will be assessed. Both CT and FRET are important for electronic and biological applications. Similar to organic photovoltaics, CT occurs as an excited electron is transferred from a donor (D) to an acceptor (A) material. Having CT ability will confirm that the molecular design for our acceptors is efficient in accepting electrons. FRET occurs when the emission from an excited state donor is absorbed by the ground state acceptor, which requires significant overlap of the donor's emission spectrum with the acceptor's absorption spectrum. Additionally, the efficiency of FRET is dependent on molecular distance of D and A with a range between 10 Å – 100 Å,[24] making 1D self-assembly ideal for creating better distance control.

This thesis will present four new molecules designed for 1D self-assembly that function as an n-type material. Using strategic molecular design, we show the control of E_{LUMO} by increasing the electron deficiency of the molecule's core structure. Following molecular design, synthetic routes to the title molecules are described and their properties are characterized using UV-Visible absorption and fluorescence emission spectroscopy, cyclic voltammetry, differential scanning calorimetry, and theoretical evaluations. For select title molecules, CT and FRET were studied using UV-Visible absorption and fluorescence emission spectroscopy, polarized optical microscopy, and organogelation.

1.2 Molecular Design

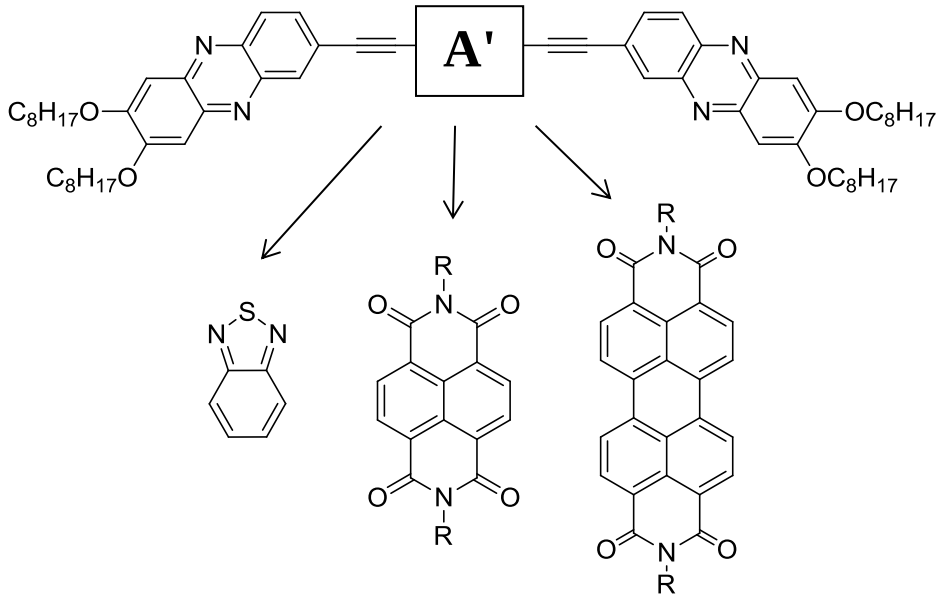

Figure 1. Design principle for title molecules.

A primary objective in molecular design is to create a material with a large electron affinity while maintaining the desired self-assembling properties. Shown in Figure 1, our molecular design will follow an acceptor-acceptor'-acceptor (A-A'-A) configuration; where A' was altered using electron deficient-structural components. Henceforth, A' is referred to as the "pendant". In this research, we choose three different moieties for the pendant while A remained as dialkoxyphenazine substituents.

Dialkoxyphenazine is known to help make fiber and has been reported to exhibit gelling properties with potential as an acid-sensor.[25] Phenazine is also electron deficient and has E_{LUMO} = -3.23 eV[26-27] which will help maintain a low E_{LUMO} for the overall molecule. The long octyloxy side groups promote solubility in common organic solvents and assist self-assembly through van der Waals interactions.[28] All pendants are connected to the dialkoxyphenazine

groups with a triple bond to force planarity. Having a planar structure helps promote self-assembly through more effective π-π interactions which could be beneficial for enhancing charge-transport properties.[13-14]

The three pendants used were benzothiadiazole (BTD), naphthalene diimide (NDI), and perylenetetracarboxylic diimide (PTCDI). As described previously, these moieties are recognized for their high electron withdrawing ability as n-type acceptors and low lying E_{LUMO}.[29-31] As the pendant is changed from BTD to NDI to PTCDI, we hope to see a decrease in the overall molecules E_{LUMO} and ultimately obtain a target E_{LUMO} similar to PCBM of -4.08 eV.[6]

2 EXPERIMENTAL

2.1 Instrumentation

Nuclear magnetic resonance (NMR) spectra were measured using a Varian Gemini 400 MHz NMR spectrometer operated at room temperature. The samples were prepared for both ^{1}H and ^{13}C NMR analysis by dissolving the compound in deuterated chloroform ($CDCl_3$) containing tetramethylsilane (TMS) as an internal standard. The chemical shifts were then reported in parts per million (ppm) relative to the internal standard (TMS; 0.0). Mass spectra were collected by the University of Texas at Arlington. Absorption and emission properties were obtained for all title molecules in both solution and solid state. The absorption properties were analyzed using a Shimadzu UV-2600 UV-visible spectrophotometer equipped with xenon lamp as the excitation source. The photoluminescent properties were analyzed using a Perkin-Elmer LS 55 luminescence spectrometer, which also used a xenon lamp as the excitation source. Phase transition temperatures of the title compounds were studied using differential scanning calorimetric (DSC) analyses on a TA instrument Q200 series DSC. Analyses were performed under nitrogen atmosphere at heating and cooling rates of 10 ^{o}C/min. The temperature axis of the

DSC thermograms was calibrated against high purity indium and tin reference standards. Thermal properties were studied by thermal gravimetric analysis (TGA) using a TA instrument Q50 series TGA. Analyses were performed under nitrogen atmosphere at a heating rate of 10 ^{o}C/min in the temperature range between 30 and 800 ^{o}C. Electrochemistry measurements were performed using cyclic voltammetry (CV) on a CHI660D from CH Instruments, Inc. The cell was equipped using a three electrode configuration; a platinum plate as the counter electrode, a platinum disc (2 mm diameter) as the working electrode, and a non-aqueous Ag/Ag^{+} electrode (Ag in 10 mM $AgNO_3$ acetonitrile solution) as the reference electrode. CV measurements for all compounds were recorded in a 25 mL methylene chloride solution containing 0.1 M tetrabutylammonium hexafluorophosphate ($TBAPF_6$) as the supporting electrolyte. The solution was purged with argon gas for 30-60 minutes before each experiment, and a positive pressure of argon flow was maintained over the sample solution during each experiment. The scan rate was set to 0.1 V/s and the sample interval was 0.001 V for all experiments. The potentials were calibrated relative to the redox couple of the internal standard, ferrocene/ferrocenium (Fc/Fc^{+}). Polarized Optical Microscopy (POM) images were obtained using a cast film from dichloromethane solution, which was evaporated onto a glass slide. The images were then captured using 100 micrometer magnification on a POM microscope.

2.2 Synthetic Procedures

All solvents and reagents were purchased from commercial vendors and used without further purification. The precursors, 1-iodo-3,4-dinotrobenzene[40] (**2**) and 1-iodobenzene-3,4-diamine[32] (**3**) were synthesized according to previously reported procedures. Additional precursors: 7-iodo-2,3-bis(hydroxyl)phenazine (**4**) and 7-triisopropylsilylethynyl-2,3-bis(octyloxy)phenazine (**6**); and intermediates: 7-iodo-2,3-bis(octyloxy)phenazine (**5**) and 7-

ethynyl-2,3-bis(octyloxy)phenazine (**7**), were prepared by the procedure shown in section 3.1 as Scheme 1. Target molecule **BTD-P**, was synthesized according to Scheme 2 in section 3.1, and the necessary precursors: 4,7-diethynyl-2,2,3-benzothiadiazole[33] (**11**) and 4,7-dibromo-2,1,3-benzothiadiazole[34] (**9**) were prepared following literature procedures. **NDI-P-1** was synthesized according to Scheme 3 in section 3.1, and the necessary precursors: 2,6-dibromo-1,4,5,8-napthalenetetracarboxylic acid dianhydride[35] (**14**) and di-(2-ethyl-1-hexyl)-2,6-dibromo1,4,5,8-napthalenetetracarboxylic acid bisimide[36] (**15**) were prepared following literature procedures. **NDI-P-2** was synthesized according to Scheme 4 in section 3.1, and the necessary precursors: 2,6-dibromo-1,4,5,8-napthalenetetracarboxylic acid dianhydride[35] (**14**) and dioctyl-2,6-dibromo1,4,5,8-napthalenetetracarboxylic acid bisimide[36] (**16**) were prepared following literature procedures. **PTCDI-P** was synthesized according to Scheme 5 in section 3.1, and the necessary precursors: 1,7-dibromopetylene-3,4:9,10-tetracarboxylic acid dianhydride[37] (**20**) and di-(2-ethyl-1-hexyl)-1,7-dibromo3,4:9,10-perylenetetracarboxylic acid bisimide[38] (**21**) were prepared following literature procedures. Chemical structures of intermediate **5**, precursor **6**, and target molecules **BTD-P**, **NDI-P-1**, **NDI-P-2** and **PTCDI-P**, were confirmed by ^{1}H NMR, ^{13}C NMR and mass spectrometry.

1-iodo-3,4-dinitrobenzene[40] (2): In a round bottom flask over ice, 1.0 g (4.02 mmol) of 1-iodo-3-nitrobenzene was dissolved in H_2SO_4 (4.2 mL), followed by fuming HNO_3 (3.1 mL). The flask was removed from the ice and placed in an oil bath set at 85^{o}C and stirred for 3 hours under nitrogen. The reaction mixture was then poured over ice water (100 mL), stirred for 10 minutes and filtered with cold water. The filter cake was left to dry for 30 minutes and then recrystallized using hot ethanol. The crystals were collected by filtering and washed with cold ethanol giving a yellow crystal solid product (41% yield).

1-iodobenzene-3,4-diamine[32] **(3):** To a flask containing 300 mg (1.02 mmol) of 1-iodo-3,4-dinitrobenzene (**2**), ethanol (6 mL) and 38% HCl (3 mL) were added and the mixture was stirred until a clear, yellow solution was obtained. 0.515 g (4.33 mmol) of Sn, metal was then added to the flask and the mixture became a dark brown/grey color which quickly turned to a bright red/orange. After about 30 minutes of mixing at room temperature, the solution became a light orange color and was left to mix another 2.5 hours. The temperature was then increased to 45^{o}C for 1.5 hours and again to 70^{o}C for 0.5 hours where the solution became clear. The flask was allowed to cool to room temperature and then poured into H_2O (100 mL). Sodium carbonate was added until the mixture was neutral. It was then extracted using ethyl acetate and H_2O where the organic layer was collected, dried over sodium sulfate, filtered, and evaporated. This gave yield to an orange solid at room temperature (96% yield).

7-iodo-2,3-bis(hydroxyl)phenazine (4): To a 1-neck round bottom flask containing 230 mg (0.98 mmol) of diamine compound (**3**), ethanol (22 mL) and 2,5-dihydroxy-1,4-benzoquinone (137 mg, 0.98 mmol) were added. The mixture was a dark red/wine colored solution. The solution was stirred at 80^{o}C for 24 hours and then cooled room temperature and connected to a rotary evaporator to evaporate solvent. This gave crude product as a dark red solid.

7-iodo-2,3-bis(octyloxy)phenazine (5): To the same flask containing an approximate 331 mg (0.98 mmol) of crude reactant **4**, dimethylformamide (22 mL), potassium carbonate (474 mg, 3.43 mmol), and 1-bromooctane (568 mg, 2.94 mmol) were added. The flask was refluxed at 60^{o}C for 48 hours under nitrogen gas. It was then cooled to room temperature, precipitated in H_2O (250 mL) and filtered. The filter cake was dissolved in $CHCl_3$, dried with sodium sulfate, attached to silica and purified by silica gel column chromatography (50% methylene chloride in hexane) providing pure product as a yellow solid (55% yield). ^{1}H NMR (400 MHz, $CDCl_3$,

ppm): δ 8.57 (1H, d, *J* = 2.0 Hz), 7.94 (1H, dd, *J* = 2.0, 1.6 Hz), 7.84 (1H, d, *J* = 8.8 Hz), 7.30 (2H, s), 4.22 (4H, td, *J* = 2.8, 2.8, 2.4 Hz), 1.95 (4H, quint, *J* = 7.0 Hz), 1.52 (4H, quint, *J* = 7.6 Hz), 1.40-1.31 (16H, m), 0.896 (6H, t, *J* = 6.8 Hz); ^{13}C NMR (100 MHz, $CDCl_3$, ppm): δ 154.96, 154.81, 142.38, 142.16, 142.10, 140.66, 137.75, 137.28, 129.92, 105.42, 105.41, 94.46, 69.33, 69.32, 31.77, 29.28, 29.22, 28.68, 25.99, 22.63, 14.07 (7 alkyl peaks not seen due to overlapping signals); HRMS (ESI) *m/z* $[M+H]^+$ calcd for $C_{28}H_{39}N_2O_2I$ 563.2129, found 563.2134.

7-triisopropylsilylethynyl-2,3-bis(octyloxy)phenazine (6): To a two-neck round bottom flask, 200 mg (0.356 mmol) of iodo-phenazine (**5**), 4.9 mg (0.007 mmol) of $Pd(PPh_3)_2Cl_2$ and 1.3 mg (0.007 mmol) of CuI were added under nitrogen atmosphere and the flask was capped with a rubber stopper. Tetrahydrofuran (4 mL) and triethylamine (1 mL) were degassed with argon for 30 minutes, and then added to the flask through the rubber stopper using a glass syringe. The resulting solution was mixed until homogeneous. Triisopropylsilyl acetylene (97 mg, 0.534 mmol) was then added with a syringe through the stopper and the solution was left to mix at 65^{o}C for 1.5 hours. After cooling, the solution was poured over a Ceelite® filter and rinsed with hot $CHCl_3$ giving a yellow filtrate solution that showed blue fluorescence. The filtrate was attached to silica and purified by silica gel column chromatography (80% methylene chloride in hexane) providing a pure yellow solid product (99% yield). ^{1}H NMR (400 MHz, $CDCl_3$, ppm): δ 8.27 (1H, d, *J* = 1.6 Hz), 8.04 (1H, d, *J* = 8.8 Hz), 7.74 (1H, dd, *J* = 1.6, 1.6 Hz), 7.31 (2H, d, *J* = 1.2 Hz), 4.23 (4H, td, *J* = 1.2, 0.8, 1.2 Hz), 1.96 (4H, quint, *J* = 6.8 Hz), 1.57-1.51 (7H, m), 1.42-1.31 (16H, m), 1.17 (18H, d, *J* = 2.4 Hz), 0.896 (6H, t, *J* = 6.8 Hz); ^{13}C NMR (100 MHz, $CDCl_3$, ppm): δ 154.78, 154.69, 142.54, 142.05, 141.47, 140.35, 132.55, 131.68, 128.69, 123.86, 106.73, 105.61, 105.55, 94.16, 69.36, 69.34, 31.82, 29.33, 29.27, 28.73, 26.04, 22.68, 18.70, 14.11, 11.35; HRMS (ESI) *m/z* $[M+H]^+$ calcd for $C_{39}H_{60}N_2O_2Si$ 617.4497, found 617.4476.

7-ethynyl-2,3-bis(octyloxy)phenazine (7): To a one-neck round bottom flask containing 218 mg (0.354 mmol) of TIPS-phenazine (**6**) dissolved in tetrahydrofuran (10 mL), 140 mg (0.443 mmol) of tetrabutylammonium fluoride trihydrate was added and the solution was left to mix at room temperature for 1 hour. The solution was then poured over H_2O (100 mL) and extracted with $CHCl_3$. The organic layer was collected, dried over sodium sulfate and attached to silica to purify using silica gel column chromatography (100% methylene chloride). This gave yield to a bright yellow solid pure product (93% yield). ^{1}H NMR (400 MHz, $CDCl_3$, ppm): δ 8.29 (1H, d, *J* = 1.6 Hz), 8.07 (1H, d, *J* = 9.2 Hz), 7.75 (1H, dd, *J* = 1.6, 1.6 Hz), 7.32 (2H, d, *J* = 1.2 Hz), 4.23 (4H, t, *J* = 6.6 Hz), 3.30 (1H, s), 1.96 (4H, quint, *J* = 7.1 Hz), 1.52 (4H, quint, *J* = 7.6 Hz), 1.40-1.31 (16H, m), 0.896 (6H, t, *J* = 6.8 Hz).

4,7-dibromo-2,1,3-benzothiadiazole[34] **(9):** To a two-neck round bottom flask containing 5.0 g (36.7 mmol) of 2,1,3-benzothiadiazole, 110.1 mmol of 48% HBr was added. The mixture was heated under nitrogen atmosphere until a stable temperature of 115^{o}C was reached. Bromine (17.5 g, 110.1 mmol) was then added to the flask through a dropping funnel over a period of 30 minutes and the flask was left to stir for 3 hours. After cooling to room temperature, the mixture was poured over H_2O (500 mL) and the precipitate was filtered, collected, and recrystallized using hot $CHCl_3$. The crystals were collected via filtration yielding a pale beige product (48% yield). ^{1}H NMR (400 MHz, $CDCl_3$, ppm): δ 7.73 (2H, s); ^{13}C NMR (100 MHz, $CDCl_3$, ppm): δ 152.93, 132.34, 113.90.

4,7-triisopropylsilylethynyl-2,1,3-benzothiadiazole (10): To a two-neck round bottom flask assembled with a condenser and nitrogen atmosphere, 300 mg (1.02 mmol) of 4,7-dibromo-2,1,3-benzothiadiazole (**9**), 24.9 mg (0.02 mmol) of $Pd(PPh_3)_4$, and 7.6 mg (0.04 mmol) of CuI were added and the flask was capped with a rubber stopper. Trimethylsilyl acetylene (301 mg,

3.06 mmol) was then added through the stopper followed by triethylamine (12 mL, degassed with argon 30 minutes). The solution was left to mix 5 hours at 75^{o}C and then cooled to room temperature and extracted with H_2O and dichloromethane. The organic layer was neutralized with 1.25N HCl, dried over sodium sulfate and then attached to silica for purification using silica gel column chromatography (30% methylene chloride in hexane). Yellow solid pure product was obtained (74% yield).

4,7-diethynyl-2,2,3-benzothiadiazole[33] **(11):** To a flask containing 248 mg (0.75 mmol) of compound **10** dissolved in CH_2Cl_2 (6 mL), potassium carbonate (311 mg, 2.25 mmol) and methanol (6 mL) were added. The solution was left to mix overnight under nitrogen atmosphere at room temperature and then filtered over Ceelite® bed and washed with hot CH_2Cl_2. The filtrate was connected to a rotary evaporator and solvent was evaporated. This gave a crude product of a yellow/brown solid (102% yield). ^{1}H NMR (400 MHz, $CDCl_3$, ppm): δ 7.77 (2H, s), 3.69 (2H, s).

BTD-P (Route 1): To a two-neck round bottom flask assembled with condenser and nitrogen atmosphere, 33 mg (0.18 mmol) of reactant **11**, 200 mg (0.36 mmol) of reactant **5**, 1.3 mg (0.002 mmol) of $Pd(PPh_3)_2Cl_2$ and 0.34 mg (0.002 mmol) of CuI were added and the flask was capped with a rubber stopper. Tetrahydrofuran (7 mL) and triethylamine (2 mL), which had previously been degassed with argon for 30 minutes, were then added to the flask via glass syringe through the rubber stopper. The mixture was refluxed for 4 hours at 80^{o}C giving a dark red solution color. After cooling to room temperature, the solution was filtered through Ceelite® and rinsed with hot $CHCl_3$. The filtrate was connected to a rotary evaporator and the solvent was evaporated. This gave very small amount of product shown on TLC, so no further purification was conducted.

BTD-P (Route 2): To a two-neck round bottom flask assembled with condenser and nitrogen atmosphere, 152 mg (0.33 mmol) of reactant **7**, 44 mg (0.15 mmol) of reactant **9**, 2.1 mg (0.003 mmol) of $Pd(PPh_3)_2Cl_2$ and 0.6 (0.003 mmol) of CuI were added and the flask was capped with a rubber stopper. Tetrahydrofuran (6 mL) and triethylamine (2 mL), which had previously been degassed with argon for 30 minutes, were then added to the flask via glass syringe through the rubber stopper. The mixture was refluxed overnight at 70^{o}C, cooled to room temperature and then placed in the fridge for 30 minutes. A dark red gel formed in the flask which was broken up using a spatula and filtered using cold methanol to help the transfer. The filter cake was dissolved in $CHCl_3$, attached to silica and purified using silica gel column chromatography (100% methylene chloride to 3% methanol in methylene chloride). The product was then re-precipitated from hot CH_2Cl_2 into methanol, filtered and collected giving a dark yellow solid (43% yield). ^{1}H NMR (400 MHz, $CDCl_3$, ppm): δ 8.46 (2H, d, *J* = 1.6 Hz), 8.14 (2H, d, *J* = 8.8 Hz), 7.95 (2H, dd, *J* = 2.0, 2.0 Hz), 7.92 (2H, s), 7.34 (4H, d, *J* = 4.4 Hz), 4.24 (8H, td, *J* = 2.8, 2.4, 2.8 Hz), 1.97 (8H, quint, *J* = 6.7 Hz), 1.53 (8H, quint, *J* = 7.2 Hz), 1.43-1.31 (32H, m), 0.903 (12H, t, *J* = 6.8 Hz). ^{12}C NMR (100 MHz, $CDCl_3$, ppm): δ 154.92, 154.72, 154.33, 142.62, 142.21, 141.67, 141.25, 132.64, 132.60, 131.33, 128.99, 122.72, 117.18, 105.58, 105.47, 97.51, 87.87, 69.37, 31.83, 29.36, 29.28, 28.77, 28.75, 26.05, 26.04, 22.68, 14.12 (6 alkyl peaks not seen due to overlapping signals); HRMS (ESI) *m/z* $[M+H]^+$ calcd for $C_{66}H_{80}N_6O_4S$ 1053.6035, found 1053.6053.

2,6-dibromo-1,4,5,8-napthalenetetracarboxylic acid dianhydride[35] **(14):** To a round bottom flask containing 1.0 g (3.73 mmol) of naphthalene dianhydride, oleum (37 mL) was added and the solution was mixed under nitrogen atmosphere until dissolved. Dibromoisocyanuric acid (1.07 g, 3.73 mmol) was dissolved in oleum (17.5 mL) and then added to the flask using a

dropping funnel over a period of 2 hours at room temperature. The resulting mixture was stirred another 2 hours and then poured over ice water (500 mL) and allowed to stand 1 hour. This formed a dark yellow precipitate which was filtered, washed with 1.25N HCl, dried and collected as the crude product (94% yield).

di-(2-ethyl-1-hexyl)-2,6-dibromo1,4,5,8-napthalenetetracarboxylic acid bisimide[36] **(15):** To a round bottom flask containing 1.26 g (2.96 mmol) of 2,6-dibromo-1,4,5,8-napthalenetetracyanuric acid (**14**), acetic acid (40 mL) was added and the mixture was heated to 120^{o}C for 20 minutes. 2-ethyl-1-hexylamine (20 mmol) was then added and the mixture continued to reflux another 20 minutes. The solution was then poured over H_2O (400 mL), which formed a light brown precipitate that was filtered, dried, and attached to silica for purification using silica gel column chromatography (60% methylene chloride in hexane). The pure product obtained was a pale yellow solid (4.7% yield). ^{1}H NMR (400 MHz, $CDCl_3$, ppm): δ 9.00 (2H, s), 4.21-4.12 (4H, m), 1.98-1.89 (2H, m), 1.41-1.28 (16H, m), 0.936 (6H, t, *J* = 7.4 Hz), 0.885 (6H, t, *J* = 7.0 Hz).

dioctyl-2,6-dibromo1,4,5,8-napthalenetetracarboxylic acid bisimide[36] **(16):** To a round bottom flask containing 2.40 g (5.63 mmol) of 2,6-dibromo-1,4,5,8-napthalenetetracyanuric acid **(14)**, acetic acid (70 mL) was added and the mixture was heated to 120^{o}C for 20 minutes. octylamine (4.91 g, 38 mmol) was then added and the mixture continued to reflux another 20 minutes. The solution was then poured over H_2O (700 mL), which formed a light brown precipitate that was filtered, dried, and attached to silica for purification using silica gel column chromatography (70% methylene chloride in hexane). The pure product obtained was a pale pink solid (4.8% yield). ^{1}H NMR (400 MHz, $CDCl_3$, ppm): δ 9.00 (2H, s), 4.19 (4H, t, *J* = 7.6 Hz), 1.73 (4H, quin, *J* = 7.5 Hz), 1.45-1.28 (20H, m), 0.880 (6H, t, *J* = 7.0 Hz).

NDI-P-1: To a round bottom flask containing 217 mg (0.471 mmol) of reactant **7**, 139 mg (0.214 mmol) of reactant **15**, 3.0 mg (0.0043 mmol) of $Pd(PPh_3)_2Cl_2$ and 0.8 mg (0.0043 mmol) of CuI were added and the flask was connected to nitrogen atmosphere and capped with a rubber stopper. Tetrahydrofuran (18 mL) and triethylamine (6 mL), which had previously been degassed with argon for 30 minutes, were then added to the flask via glass syringe through the rubber stopper. The mixture was stirred at room temperature for 1.5 hours and then methanol (20 mL) was added to the flask allowing precipitation. The flask was placed in the fridge for 1 hour and then filtered using cold methanol to help the transfer. The filter cake was dissolved in $CHCl_3$ and attached to neutral alumina for purification with neutral alumina column chromatography (100% chloroform). It was then attached to basic alumina for further purification using basic alumina column chromatography (20% ethyl acetate in hexane). The collected product was re-precipitated from hot CH_2Cl_2 into methanol and filtered. Filter cake was collected and dried giving product as dark red solid (64% yield). ^{1}H NMR (400 MHz, $CDCl_3$, ppm): δ 8.76 (2H, s), 8.43 (2H, d, *J* = 1.6 Hz), 8.07 (2H, d, *J* = 8.8 Hz), 7.98 (2H, dd, *J* = 1.6, 1.6 Hz), 7.27 (2H, s), 7.24 (2H, s), 4.30-4.18 (12H, m), 2.11-2.03 (2H, m), 1.99 (4H, quint, *J* = 7.2 Hz), 1.90 (4H, quint, *J* = 7.2 Hz), 1.62-1.25 (56H, m), 1.03 (6H, t, *J* = 7.4 Hz), 0.97-0.87 (18H, m). ^{13}C NMR (100 MHz, $CDCl_3$, ppm): δ 161.83, 160.93, 154.89, 154.49, 141.98, 141.73, 141.28, 140.51, 135.66, 133.26, 131.59, 128.67, 125.43, 125.02, 124.50, 123.90, 122.89, 105.35, 105.12, 101.95, 92.08, 69.28, 69.17, 44.54, 37.94, 31.92, 31.82, 30.77, 29.46, 29.40, 29.37, 29.24, 28.93, 28.75, 26.15, 25.86, 24.02, 23.29, 22.74, 22.64, 14.33, 14.16, 14.09, 10.77 (1 alkyl peak not seen due to overlapping signals); HRMS (ESI) *m/z* $[M+H]^+$ calcd for $C_{90}H_{114}N_6O_8$ 1407.8771, found 1407.8769.

NDI-P-2: To a round bottom flask containing 54 mg (0.117 mmol) of reactant **7**, 34 mg (0.053 mmol) of reactant **16**, 0.7 mg (0.001 mmol) of $Pd(PPh_3)_2Cl_2$ and 0.2 mg (0.001 mmol) of CuI were added and the flask was connected to nitrogen atmosphere and capped with rubber stopper. Tetrahydrofuran (4.5 mL) and triethylamine (1.5 mL), which had previously been degassed with argon for 30 minutes, were then added to the flask via glass syringe through the rubber stopper. The mixture was stirred at room temperature for 2.5 hours and then methanol (10 mL) was added to the flask allowing precipitation. The flask was placed in the fridge for 1 hour and then filtered using cold methanol to help the transfer. The filter cake was dissolved in $CHCl_3$ and attached to neutral alumina for purification with neutral alumina column chromatography (100% chloroform). The collected product was re-precipitated from hot CH_2Cl_2 into methanol and filtered. Filter cake was collected and dried giving product as dark red solid (54% yield). ^{1}H NMR (400 MHz, $CDCl_3$, ppm): δ 8.59 (2H, s), 8.32 (2H, s), 7.98 (2H, d, *J* = 8.8 Hz), 7.91 (2H, dd, *J* = 1.6, 1.6 Hz), 7.19 (2H, s), 7.13 (2H, s), 4.28-4.21 (8H, m), 4.13 (4H, t, *J* = 6.6 Hz), 1.98 (4H, quint, *J* = 7.5 Hz), 1.91-1.80 (8H, m), 1.52-1.26 (60H, m), 0.93-0.86 (18H, m). ^{13}C NMR (100 MHz, $CDCl_3$, ppm): δ 161.36, 160.50, 154.84, 154.47, 142.02, 141.79, 141.32, 140.48, 135.77, 133.45, 131.40, 128.69, 125.53, 125.25, 124.59, 124.07, 122.60, 105.31, 105.10, 101.90, 91.87, 69.22, 69.15, 41.08, 31.95, 31.87, 31.79, 29.50, 29.44, 29.36, 29.32, 29.22, 28.87, 28.72, 28.13, 27.35, 26.12, 25.86, 22.74, 22.69, 22.61, 14.16, 14.11, 14.05 (1 alkyl peak not seen due to overlapping signals). HRMS (ESI) *m/z* $[M+H]^+$ calcd for $C_{90}H_{114}N_6O_8$ 1407.8771, found 1407.8791.

1,7-dibromopetylene-3,4:9,10-tetracarboxylic acid dianhydride[37] **(20):** To a round bottom flask containing 2.0 g (5.09 mmol) of perylene-3,4:9,10-tetracarboxylic acid dianhydride (**19**), H_2SO_4 (60 mL) was added and the mixture was left to stir at room temperature for 1 hour. Iodine

(103 mg, 0.4 mmol) was then added and the solution was heated to 85°C over 45 minutes. Bromine (4.87 g, 30.5 mmol) was then added and the mixture was stirred overnight at 95°C. After cooling to room temperature, the solution was poured into H_2O (600 mL) and the precipitate was filtered. The filter cake was collected and dried giving a rust-colored crude product.

di-(2-ethyl-1-hexyl)-1,7-dibromo3,4:9,10-perylenetetracarboxylic acid bisimide[38] **(21):** To a round bottom flask containing 1.0 g (1.82 mmol) of 1,7-dibromoperylene-3,4,9,10-tetracarboxylic acid dianhydride (**20**), a solution of *n*-butyl alcohol (35 mL) and water (35 mL) was added and the flask was sonicated for 10 minutes. 2-ethyl-1-hexylamine (823 mg, 6.37 mmol) was then added and the reaction mixture was stirred for 24 hours at 80°C. Concentrated HCl (7 mL) was then added and the mixture was stirred at room temperature for 30 minutes. The mixture was extracted with $CHCl_3$, washed with water, dried with $MgSO_4$, and connected to a rotary evaporator to evaporate solvent. The product was then re-precipitated from hot $CHCl_3$ into methanol, filtered, collected and attached to silica for purification with silica gel column chromatography (70% chloroform in hexane). The collected product was re-precipitated again from hot $CHCl_3$ into methanol, filtered and dried, giving pure product as bright red solid (20% yield). ^{1}H NMR (400 MHz, $CDCl_3$, ppm): δ 9.40 (2H, d, *J* = 8.0 Hz), 8.85 (2H, s), 8.62 (2H, d, *J* = 8.4 Hz), 4.19-4.09 (4H, m), 1.99-1.89 (2H, m), 1.42-1.32 (16H, m), 0.950 (6H, t, *J* = 7.4 Hz), 0.901 (6H, t, *J* = 7.0 Hz).

PTCDI-P: To a two-neck round bottom flask containing 236 mg (0.512 mmol) of reactant **7**, 158 mg (0.205 mmol) of reactant **21**, 5.8 mg (0.0082 mmol) of $Pd(PPh_3)_2Cl_2$ and 1.6 mg (0.0082 mmol) of CuI were added and the flask was connected to nitrogen atmosphere and capped with a rubber stopper. Tetrahydrofuran (12 mL) and triethylamine (4 mL), previously degassed with

argon for 30 minutes, where then added to the flask via glass syringe through the rubber stopper. The solution was stirred at room temperature for 5 hours and then precipitated by adding methanol (20 mL) and placed in the fridge for 30 minutes. The precipitate was filtered, washed with cold methanol, collected, dissolved in $CHCl_3$ and attached to silica for purification with silica gel column chromatography (70% chloroform in hexane to 0.5% methanol in chloroform). The product was then attached to neutral alumina for further purification using neutral alumina column chromatography (70% chloroform in hexane to 100% chloroform). The collected product was re-precipitated from hot $CHCl_3$ into methanol, filtered, dried and collected as a dark purple/black solid (28% yield). ^{1}H NMR (400 MHz, $CDCl_3$, ppm): δ 9.79 (2H, d, *J* = 8.4 Hz), 8.64 (2H, s), 8.53 (2H, d, *J* = 8.0 Hz), 7.96 (2H, d, *J* = 1.6 Hz), 7.88 (2H, d, *J* = 8.4 Hz), 7.64 (2H, dd, *J* = 2.0, 1.6 Hz), 7.06 (2H, s), 6.93 (2H, s), 4.30-4.09 (12H, m), 2.03-1.92 (10H, m), 1.60-1.35 (56H, m), 1.03 (6H, t, *J* = 7.2 Hz), 0.98-0.92 (18H, m). ^{13}C NMR (100 MHz, $CDCl_3$, ppm): δ 162,94, 162.70, 154.67, 154.32, 142.05, 141.73, 141.12, 140.36, 137.20, 132.97, 132.71, 132.51, 129.94, 129.80, 129.38, 126.86, 126.45, 122.72, 121.67, 121.55, 119.53, 105.30, 105.01, 98.87, 93.20, 69.25, 69.16, 44.41, 38.05, 31.94, 31.93, 30.94, 29.57, 29.42, 29.40, 29.02, 28.97, 28.86, 26.19, 26.14, 24.16, 23.20, 22.76, 22.74, 14.23, 14.16, 14.15, 10.66 (1 aromatic peak and 1 alkyl peak not seen due to overlapping signals); HRMS (ESI) *m/z* $[M+H]^+$ calcd for $C_{100}H_{118}N_6O_8$ 1531.9084, found 1531.9110.

2.3 Organogelation

In a 4 mL screw cap vial, a known concentration of compound was suspended in a 1,1,1-Trichloroethane (TCE) solution. The vial containing the suspension was heating until the compound dissolved and then left undisturbed to cool to room temperature. When turning the vial upside down, successful gelation was identified if there was no streaming solvent.[39]

2.4 Cast Film Preparation

A known concentration of compound was dissolved in an organic solvent, forming a homogeneous solution. The solution was drop-cast onto a clean glass cover slide and left undisturbed until the solvent fully evaporated.

3 RESULTS AND DISCUSSION

3.1 Synthesis

The route to the synthesis of the final compounds **BTD-P**, **NDI-P-1**, **NDI-P-2**, and **PTCDI-P** are summarized in Scheme 2, Scheme 3, Scheme 4, and Scheme 5, respectively. All reaction schemes used a Sonogashira coupling reaction with intermediate **7** (7-ethynyl-2,3-bis(octyloxy)phenazine) and dibromo-A' (A' = BTD, NDI, and PTCDI). Meanwhile, **BTD-P** also used intermediate **5** (7-iodo-2,3-bis(octyloxy)phenazine). The synthetic route to the crucial intermediates **5** and **7** are shown in Scheme 1.

The first step in synthesizing the crucial intermediates was nitration of m-iodonitrobenzene.[40] This nitration reaction yielded 1-iodo-3,4-dinitrobenzene (**2**) which was then reduced using Sn over HCl to yield the first listed precursor; 1-iodobenzene-3,4-diamine (**3**).[32] Precursor **3** was suspended in EtOH and cyclized using 2,5-dihydroxy-1,4-benzoquinone. This cyclization reaction produced 7-iodo-2,3-bis(hydroxyl)phenazine (**4**). Compound **4** showed strong hydrogen-bonding with silica gel due to the presence of OH groups. Purification using column chromatography could not be performed. Thus, crude reactant **4** was subjected to Williamson Ether synthesis using 1-bromooctane in a dimethylformamide solution. This yielded intermediate **5**, the first crucial intermediate. Intermediate **5** was then used in a Sonogashira coupling reaction with triisopropylsilyl acetylene to yield 7-triisopropylsilylethynyl-2,3-bis(octyloxy)phenazine (**6**). Then triisopropylsilyl of compound **6** was removed using

tetrabutylammonium floride trihydrate in a tetrahydrofuran solution to yield intermediate **7**, the second crucial intermediate.

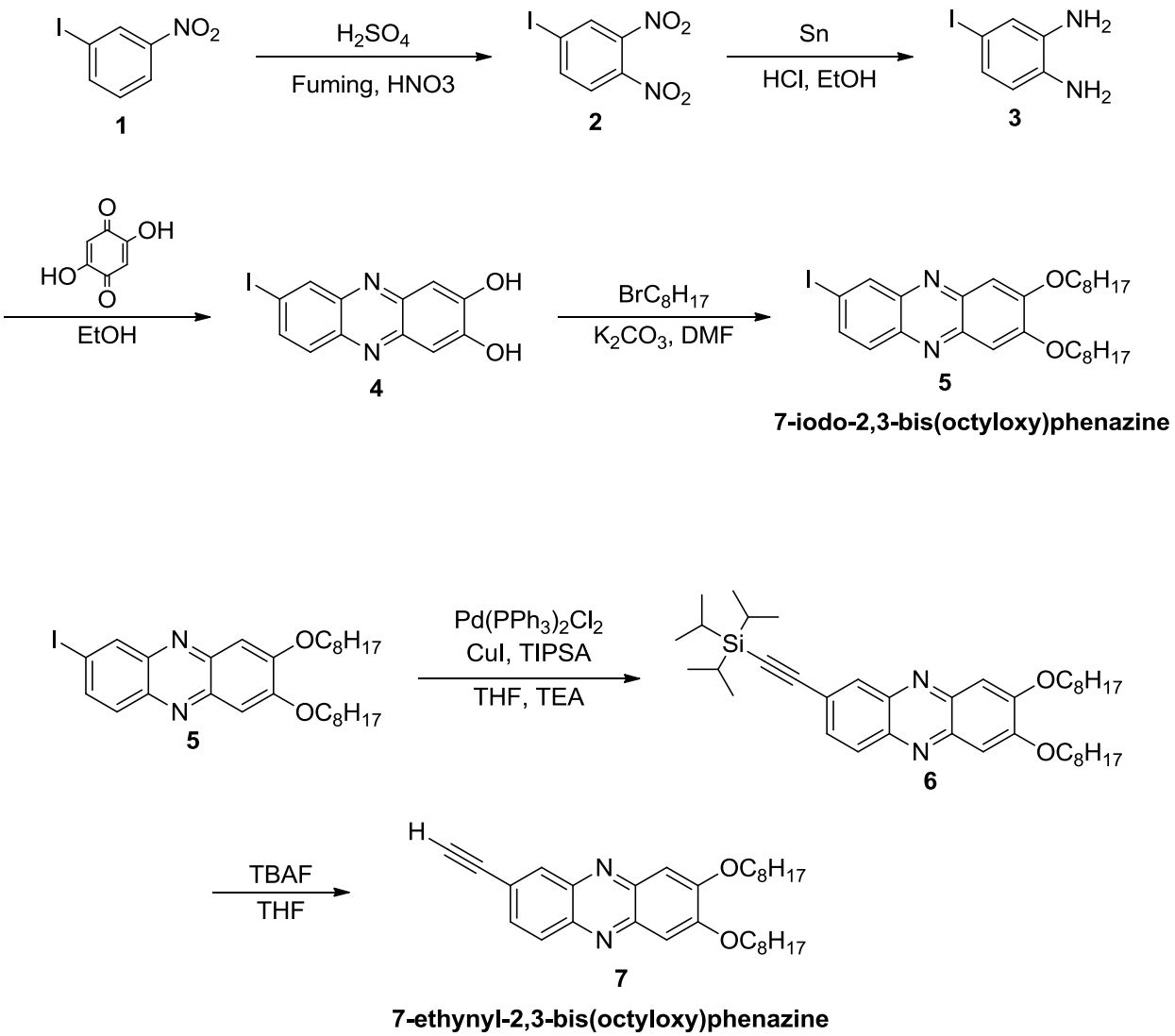

Scheme 1. Synthetic route to intermediates: 7-iodo-2,3-bis(octyloxy)phenazine (**5**) and 7-ethynyl-2,3-bis(octyloxy)phenazine (**7**).

Both intermediates (**5** and **7**) were essential to finding an efficient synthetic route for the title compounds. Scheme 2 illustrates how each intermediate was used in the synthesis of **BTD-P** following two different routes. Route 1 used intermediate **5**; while route 2 used intermediate **7**. Both routes followed a Sonogashira coupling reaction between an aryl halide and terminal alkyne. However, the structure (either phenazine or pendant) for which the aryl halide or terminal alkyne is attached switched. Route 1 used intermediate **5** as the aryl halide (phenazine structure), and reactant **11** (pendant structure, BTD) as the terminal alkyne. After reacting four hours at 80 ^{o}C, thin layer chromatography results showed very low conversion of our desired product, so the reaction was stopped and purification was not attempted. Instead, route 2 was tried by switching the substituents on the reactants. This route used dibromo-BTD (**9**) and intermediate **7**. After checking thin layer chromatography results, a much more appreciable conversion was seen for route 2 compared to route 1. Thus, the title compound **BTD-P** was obtained after silica gel column chromatography purification with a 43% yield.

A possible explanation as to why route 2 gave a more efficient conversion compared to route 1 could be due to the inductive effect and stronger polarization from BTD compared to phenazine. Therefore, compound **11** would oxidize faster leading to a lower yield as a result of degradation. An additional explanation could be because of faster decomposition with compound **11** due to the extra proton. Based on the finding that route 2 gave a more efficient conversion when synthesizing **BTD-P**, intermediate **7** was used as the terminal alkyne reactant in the final Sonogashira coupling reaction step for all additional title compounds.

Route 1

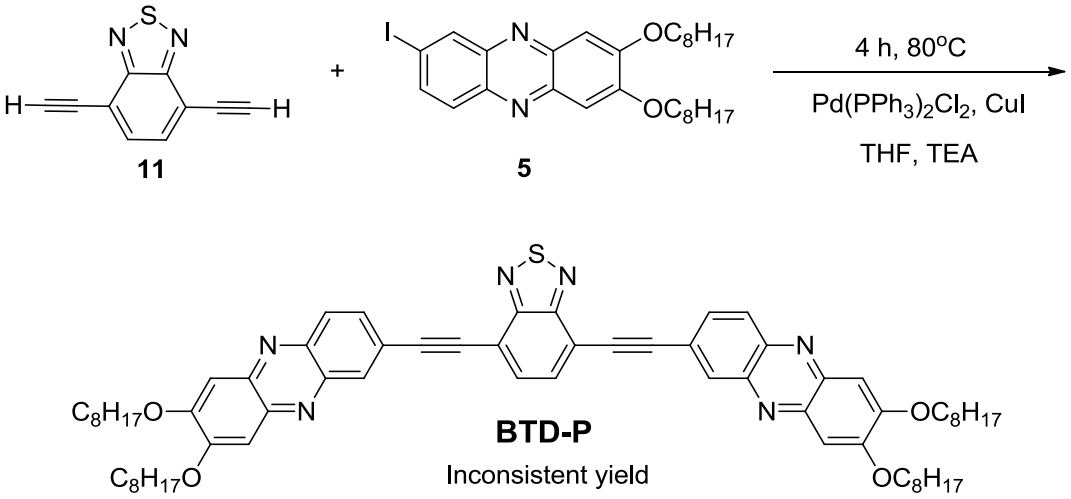

Route 2

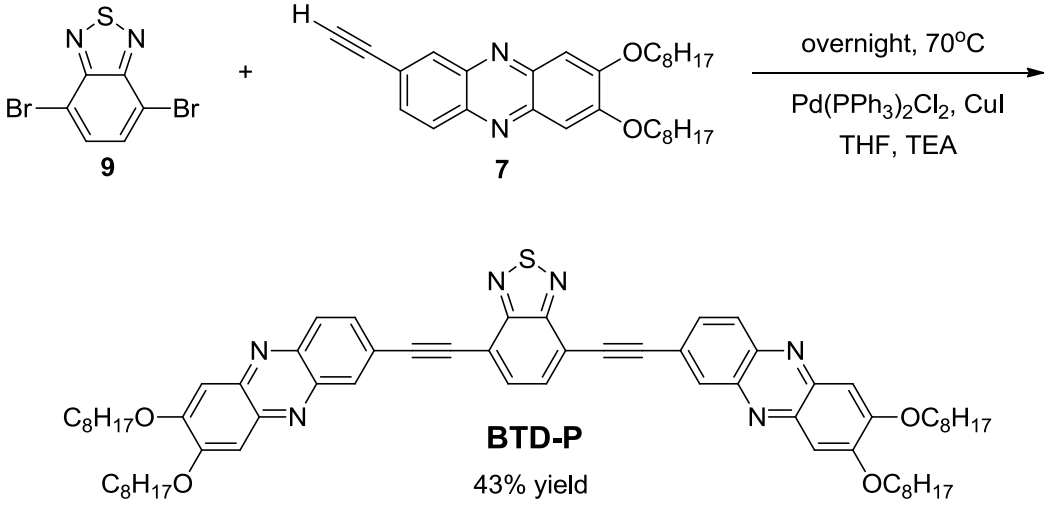

Scheme 2. Synthetic routes to the target molecule, **BTD-P**.

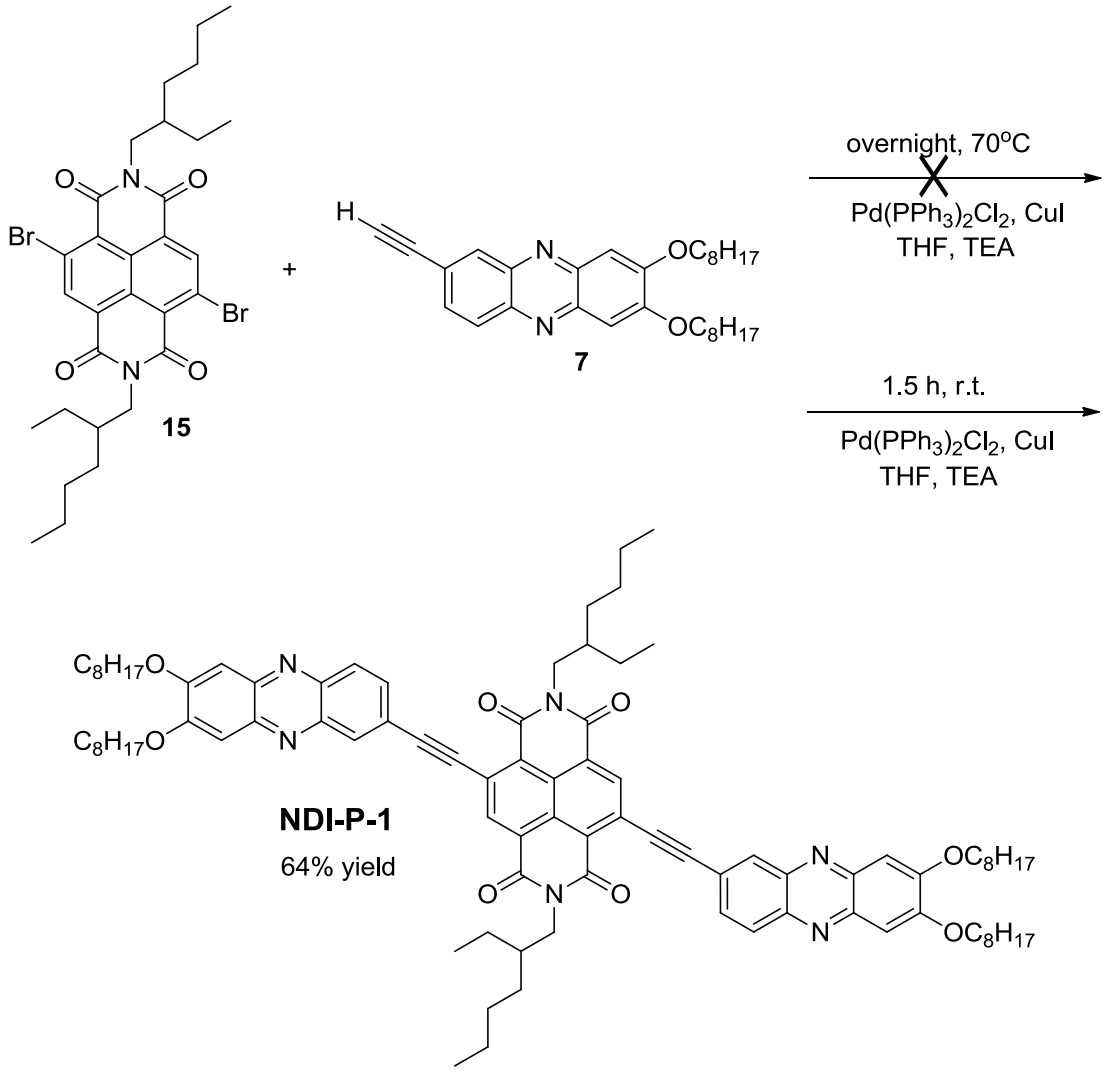

Scheme 3. Synthetic route to the target molecule, **NDI-P-1**.

The synthetic route to target molecule **NDI-P-1** is summarized in Scheme 3. This reaction scheme started with bromination of naphthalene dianhydride using dibromoisocyanuric acid and oleum to yield 2,6-dibromo-1,4,5,8-napthalenetetracarboxylic acid dianhydride (**14**).[35] Then, di-(2-ethyl-1-hexyl)-2,6-dibromo1,4,5,8-napthalenetetracarboxylic acid bisimide (**15**) was obtained through imidization reaction between 2-ethyl-1-hexylamine and dibromo-naphthalene dianhydride (**14**).[36] The final reaction step used Sonogashira coupling between intermediate **7** and reactant **15** to produce the title compound, **NDI-P-1**. This reaction required careful

optimization. Scheme 3 shows that two reaction conditions were attempted. Both reactions used the same reagents, but differed in reaction time and temperature. The first reaction condition was the same as route 2 used for **BTD-P** in Scheme 2. This route proceeded by reacting overnight at a temperature of 70 ^{o}C. Just as the reaction began, the solution turned a bright red color that appeared to be a successful conversion. However, after continuing the reaction overnight, the solution color turned dark brown. When checking thin layer chromatography results, it was seen that any possible product (red solid) had decomposed. Our hypothesis was that the reaction was sensitive to time and temperature. Therefore, the second trial was carried out at room temperature and monitored using thin layer chromatography so that the reaction could be stopped before decomposition. Maximum conversion was shown after 1.5 hours and the reaction was stopped. **NDI-P-1** could then be purified using silica gel column chromatography which gave a yield of 64%.

The synthetic route to target molecule **NDI-P-2** is summarized in Scheme 4. Following the routes to **NDI-P-1**, this reaction scheme also started with bromination of naphthalene dianhydride using dibromoisocyanuric acid and oleum to yield 2,6-dibromo-1,4,5,8-naphalenetetracarboxylic acid dianhydride (**14**).[35] Then, dioctyl-2,6-dibromo1,4,5,8-napthalenetetracarboxylic acid bisimide (**16**) was obtained through imidization reaction between octylamine and dibromo-naphthalene dianhydride (**14**).[36] The final reaction step used Sonogashira coupling between intermediate **7** and reactant **16** to produce the title compound, **NDI-P-2**. Since the only difference in molecular structure between **NDI-P-1** and **NDI-P-2** is their alkyl chain on the imide nitrogen, similar reaction conditions were followed in the final Sonogashira coupling step. After reacting 2.5 hours at room temperature, maximum product

conversion was seen based on thin layer chromatography analysis. **NDI-P-2** was purified using silica gel column chromatography which gave a yield of 54%.

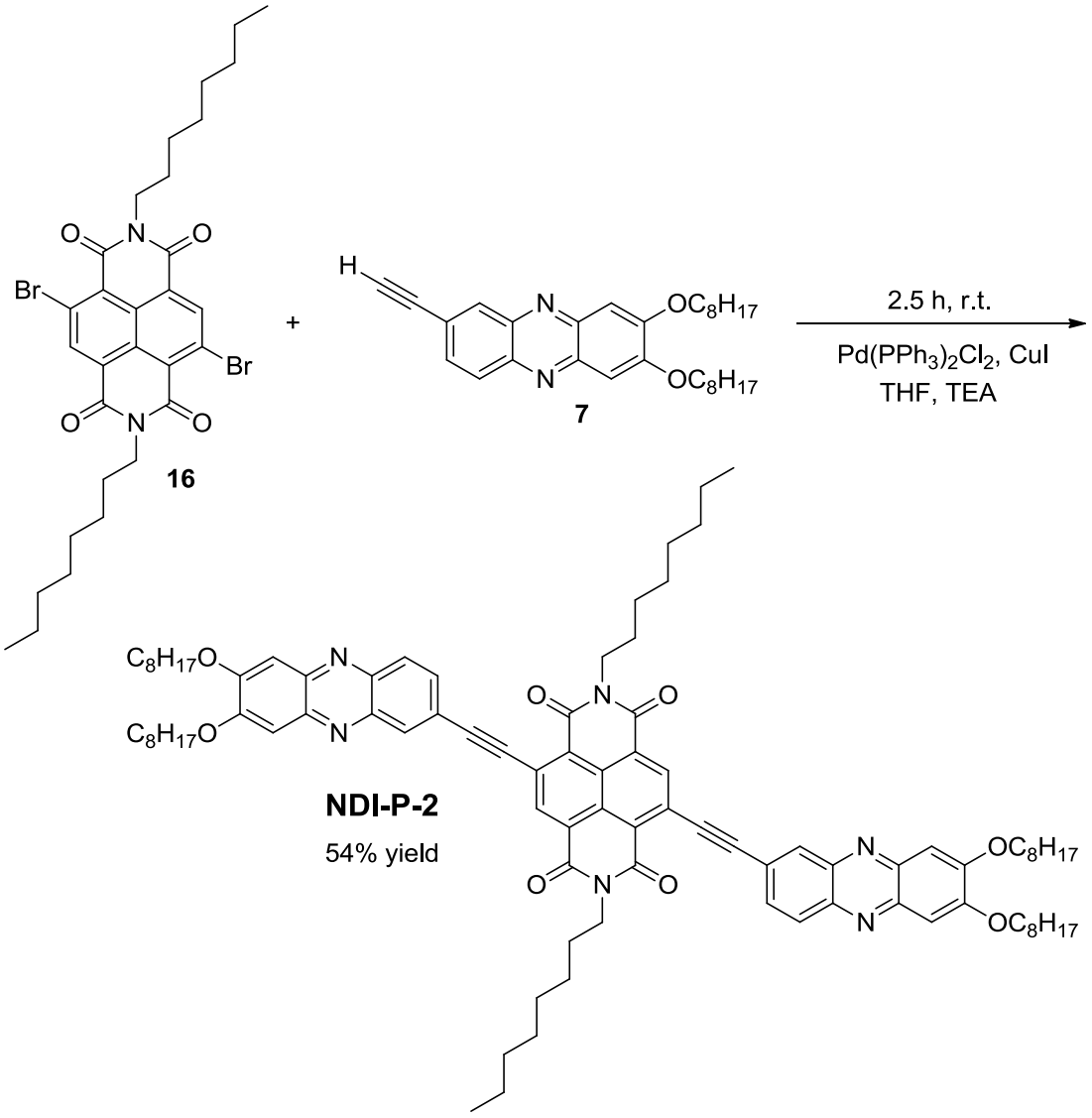

Scheme 4. Synthetic route to the target molecule, **NDI-P-2.**

An interesting comparison can be made based on experimental differences in solubility between **NDI-P-1** and **NDI-P-2**. Although both dissolved in chloroform and dichloromethane, it was expected that **NDI-P-1** would show better solubility based on the bulkiness of the alkyl

chain on the imide nitrogen which can reduce strong π-aggregation. However, **NDI-P-2** showed the better solubility. **NDI-P-2** has a longer alkyl chain, but it is straight and less bulky. Based on this observation, the length of alkyl chain may contribute to solubility more than chain bulkiness.

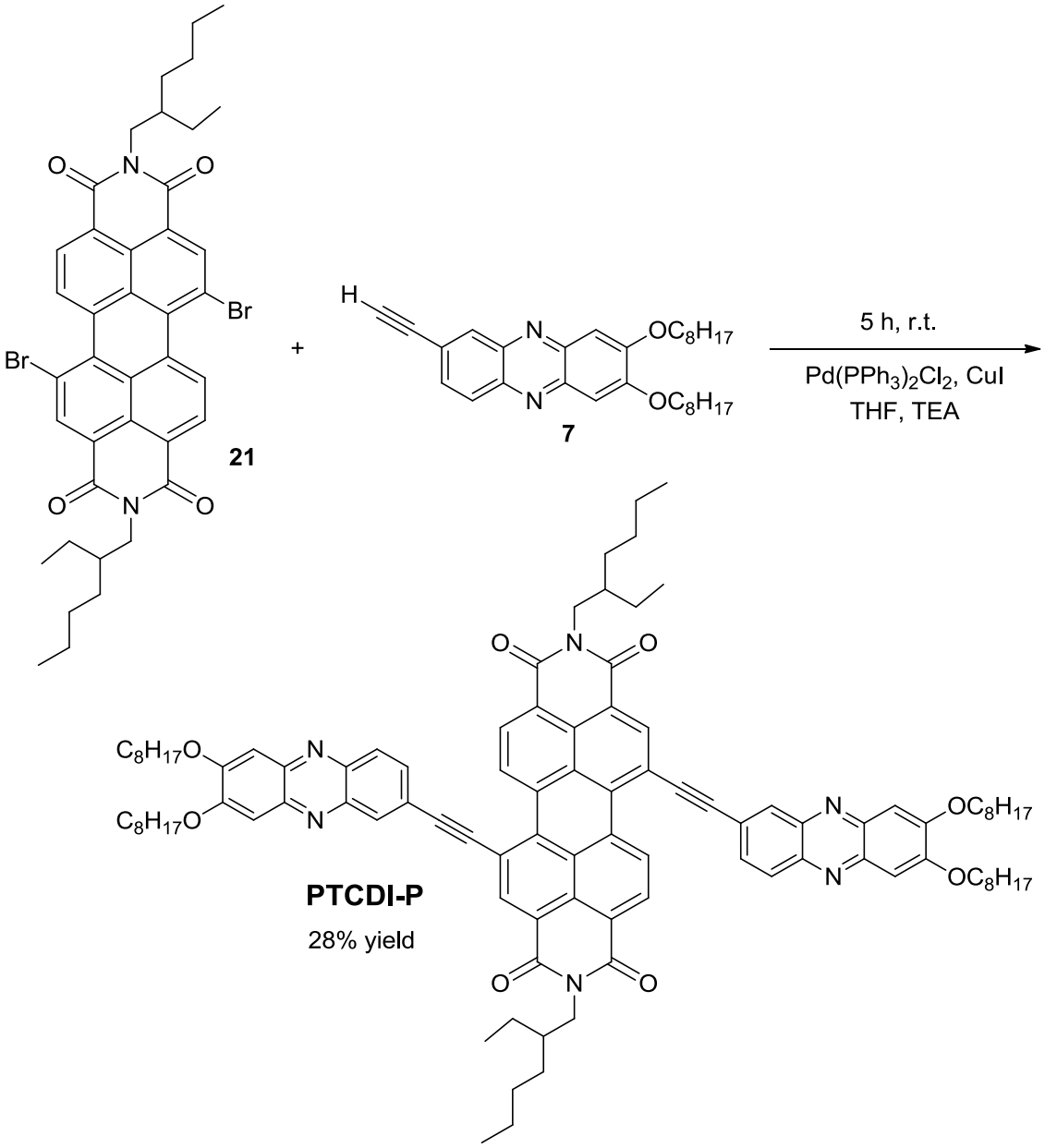

Scheme 5. Synthetic route to the target molecule, **PTCDI-P**.

The synthetic route to title compound, **PTCDI-P**, is summarized in Scheme 5. This reaction scheme started with bromination of perylene-3,4:9,10-tetracarboxylic acid dianhydride to yield 1,7-dibromopetylene-3,4:9,10-tetracarboxylic acid dianhydride (**20**).[37] Then, di-(2-ethyl-1-hexyl)-1,7-dibromo3,4:9,10-perylenetetracarboxylic acid bisimide (**21**) was obtained through imidization reaction between 2-ethyl-1-hexylamine and dibromo-perylene dianhydride (**20**).[38] The final reaction step used Sonogashira coupling between intermediate **7** and reactant **21** to produce the title compound, **PTCDI-P**. This coupling reaction was carried out under room temperature conditions showing an appreciable conversion based on thin layer chromatography analysis after 5 hours. Purification of **PTCDI-P** was extremely difficult requiring both silica gel and neutral alumina column chromatography, with a yield of 28%.

The structures and purity of **BTD-P**, **NDI-P-1**, **NDI-P-2**, and **PTCDI-P** were confirmed by ^{1}H NMR, ^{13}C NMR, and mass spectrometry.

3.2 Optical Properties

3.2.1 UV-Visible Absorption Spectroscopy

The UV-visible absorption spectra were obtained for all title compounds in both solution and solid state. The solution samples were prepared in dichloromethane with concentrations varying from 1 μM to 5 μM. The spectra shown in Figure 2 compare the absorption patterns for all compounds at 5 μM concentration. The longest wavelength absorption (λ_{max}) for **BTD-P** is observed at 445 nm. As we increase the size and electron deficiency of the pendant, λ_{max} for **NDI-P-1** and **NDI-P-2** shows longer wavelength absorption at 514 nm. Again, as the pendant continues to become more electron deficient, λ_{max} for **PTCDI-P** is further shifted to 587 nm. Thus, red-shift in the absorption occurs as electron-deficiency of pendant of the title molecules increases. Red-shift in the absorption can be translated as a reduced HOMO-LUMO energy gap

(E_{gap}). Whether the electron-deficiency of pendant plays the major role in the reduction of E_{gap} will be investigated in greater detail. It should be noted that the absorption patterns of **NDI-P-1** and **NDI-P-2** are essentially identical. This suggests that the alkyl chain does not contribute to the absorption.

Also shown in Figure 2, is that all title compounds have a second absorption peak at a shorter wavelength correlating to the dialkoxyphenazine substituents. This can be determined from the literature absorption λ_{max} for dialkoxyphenazine, which is seen at 395 nm.[41]

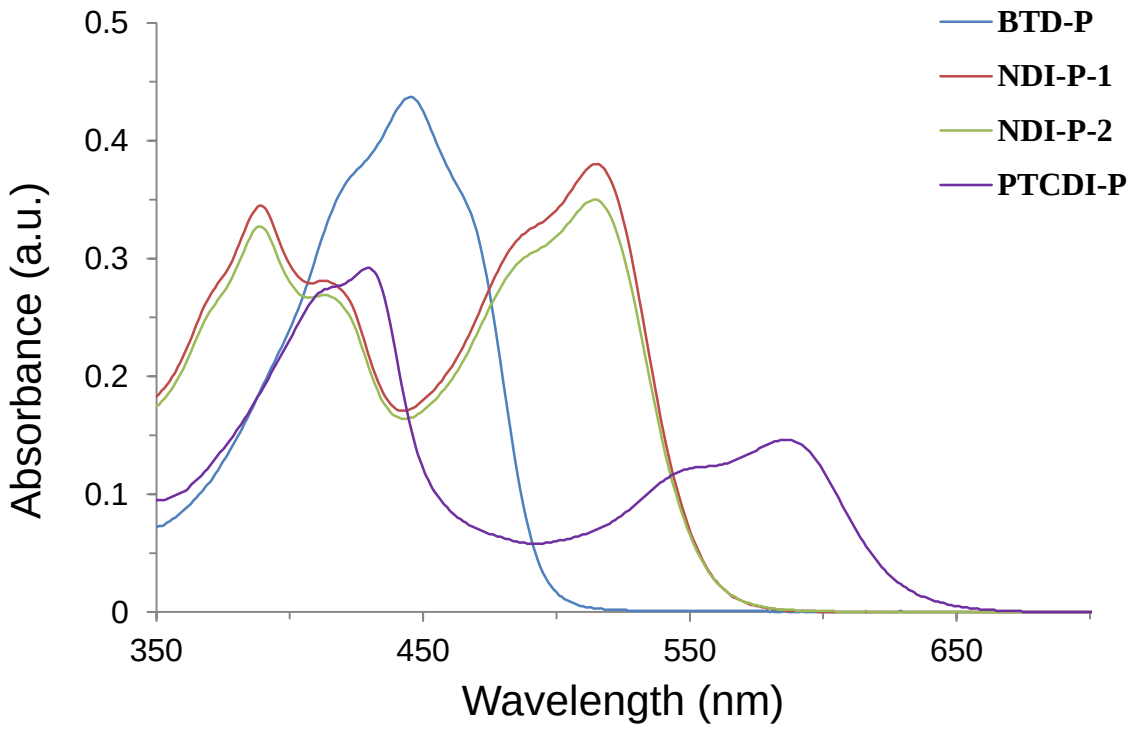

Figure 2. UV-Visible absorption spectra for **BTD-P**, **NDI-P-1**, **NDI-P-2**, and **PTCDI-P** recorded in dichloromethane with the concentration of 5 μM.

To confirm that absorption shown in Figure 2 is free of aggregation, conforming Beer's Law was tested at the concentrations of 1 μM, 2 μM, 3 μM, 4 μM, and 5 μM in dichloromethane.

Shown in Figure 3 are the linear relationships fitting with Beer's Law. This verifies the light absorbed by each solution is from isolated chromophores rather than molecular aggregations.

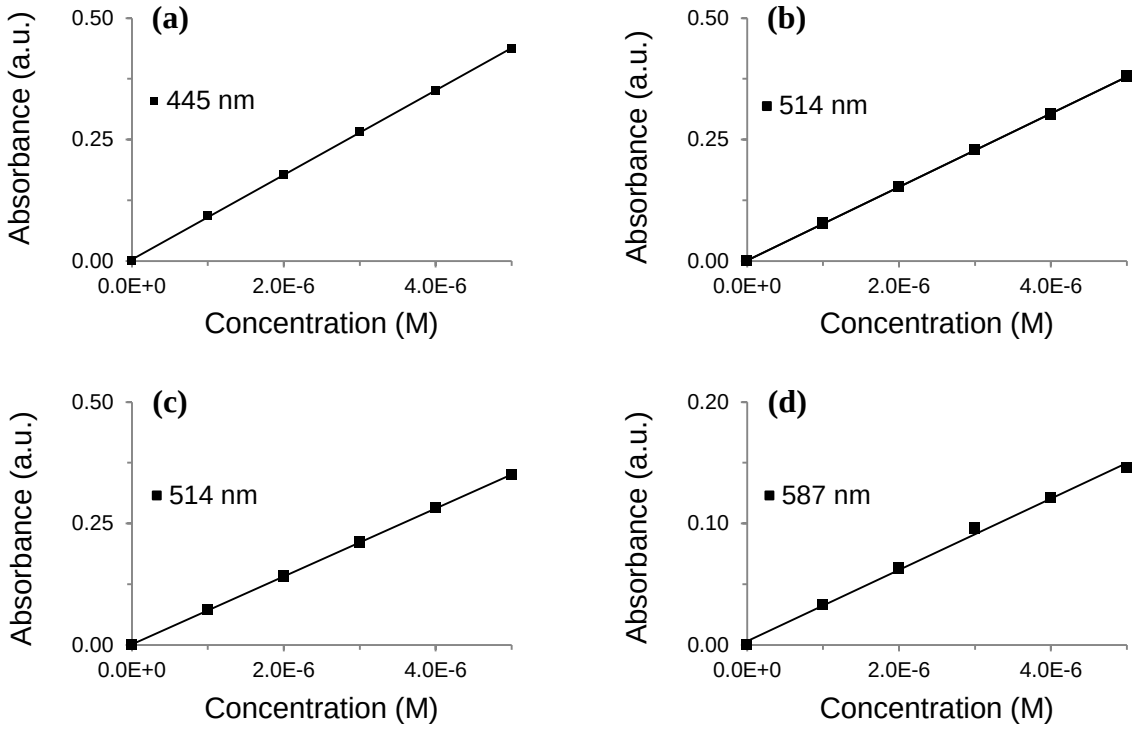

Figure 3. Beer's Law plots showing absorbance as a function of solution concentration for (a) **BTD-P**, (b) **NDI-P-1**, (c) **NDI-P-2**, and (d) **PTCDI-P**. λ_{max} at each concentration (symbol) and fitting with Lambert Beer's Law (solid line).

The molar absorptivity (ε) for the title compounds were calculated from the slope of the Beer's Law plots. These values are displayed in Table 1. **BTD-P** showed the highest absorptivity with $\varepsilon = 8.7\times10^4$ M^{-1} cm^{-1}. Similarly, **NDI-P-1** and **NDI-P-2** showed a high absorptivity of $\varepsilon = 7.6\times10^4$ M^{-1} cm^{-1} and $\varepsilon = 7.0\times10^4$ M^{-1} cm^{-1}, respectively. However, the molar absorptivity for **PTCDI-P** was much lower with $\varepsilon = 2.9\times10^4$ M^{-1} cm^{-1}.

Table 1. Molar absorptivity (ε) of title compounds at λ_{max}.

	ε (M^{-1} cm^{-1})	**λ_{max} (nm)**
BTD-P	8.7×10^4	445
NDI-P-1	7.6×10^4	514
NDI-P-2	7.0×10^4	514
PTCDI-P	2.9×10^4	587

The absorption edge area is a point of interest because it can be used to determine the energy gap between HOMO and LUMO of the molecule. As the absorption edge is shifting to longer wavelengths, the resulting E_{gap} decreases in the same order. These levels are estimated by fitting a tangent to the absorption edge and using the equation, ($E_g^{opt} = \frac{hc}{\lambda}$); where h = planks constant (6.626 x 10^{-34} Joules sec), c = speed of light (3.0 x 10^8 meter/sec), and λ = wavelength from tangent of absorption edge. Using 1 eV = 1.6 x 10^{-19} Joules as a conversion factor, the equation can be simplified to ($E_g^{opt} = \frac{1242}{\lambda}$) and the energy gap ($E_g^{opt}$) can easily be determined. The calculated values for E_g^{opt} of the title molecule using this equation are summarized in Table 2. A trend in smaller E_g^{opt} is seen as the electron affinity of the pendent increases. Therefore, **BTD-P** having the least electron deficient pendant gives the largest E_g^{opt} of 2.51 eV. Title molecules **NDI-P-1** and **NDI-P-2** with more electron deficient pendants then have E_g^{opt} of 2.23 eV. The title molecule with the most electron deficient pendent, **PTCDI-P**, gives the smallest E_g^{opt} of 1.97 eV.

Table 2. UV-Vis absorption edge and calculated band gap energy for all title compounds.

	Absorption Edge (nm)	**Band Gap Energy (E_g^{opt}; eV)**
BTD-P	494	2.51
NDI-P-1	556	2.23
NDI-P-2	556	2.23
PTCDI-P	629	1.97

Additional UV-Visible absorption spectra were obtained for the title compounds in the solid-state. These samples were prepared as a cast film from dichloromethane solution. Their resulting spectra were compared with those in the solution state as shown in Figure 4. It can be seen that the cast film spectra for the title compounds showed similar absorption patterns as their solution spectra when the pendant changed from BTD to NDI to PTCDI. However, all the cast film spectra show that λ_{max} has been significantly red-shifted from their respective solution spectrum, which is attributed to the formation of *J*-aggregates.[42] For **BTD-P**, a 27 nm red-shift was seen from the shoulder peak of λ_{max} at 462 nm in solution to 489 nm in solid phase. For **NDI-P-1** and **NDI-P-2**, a 31 nm red-shift was seen in λ_{max} at 514 nm in solution to 545 nm in solid phase. The largest red-shift of 36 nm was seen for **PTCDI-P** with λ_{max} at 587 nm in solution to 623 nm in solid phase. The *J*-aggregates in the solid-state strongly supports intermolecular π-π interactions.

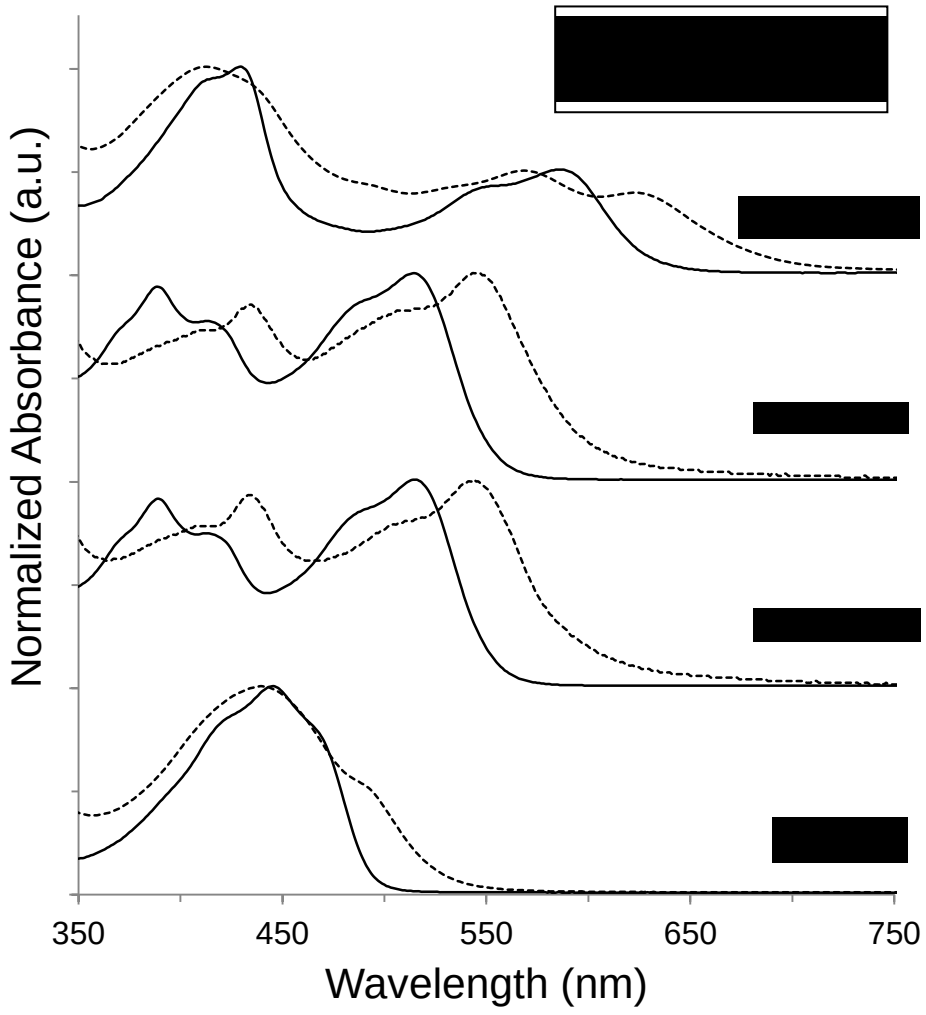

Figure 4. Normalized UV-Visible absorption spectra of **BTD-P**, **NDI-P-1**, **NDI-P-2**, and **PTCDI-P** in CH_2Cl_2 solution (solid line) and cast film from CH_2Cl_2 (dotted line).

3.2.2 Fluorescence Spectroscopy

The fluorescence spectra were obtained for **BTD-P**, **NDI-P-1**, **NDI-P-2** and **PTCDI-P** in dichloromethane. The spectra shown as Figure 5 compare the fluorescence emission maxima (λ_{em}) of the title compounds when excited at their respective λ_{max}. The measured concentrations varied according to strength of fluorescence, but remained within the concentration range that follows Lambert Beer's Law to avoid emission from aggregates. Measurement for **BTD-P** was at

a concentration of 1 μM in dichloromethane, while **NDI-P-1**, **NDI-P-2**, and **PTCDI-P** were all at 5 μM in dichloromethane. The resulting spectra were normalized for better comparison.

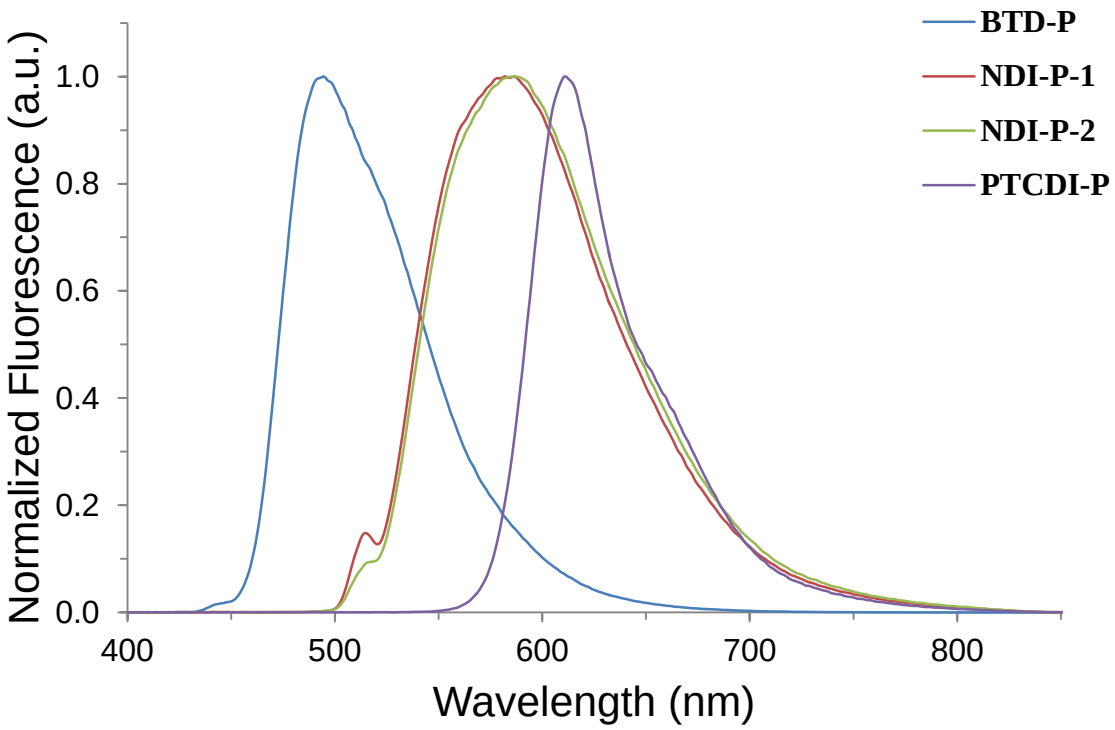

Figure 5. Normalized emission spectra of title compounds in dichloromethane solution. Excitation wavelength: 445 nm (**BTD-P**); 514 nm (**NDI-P-1** and **NDI-P-2**); 587 nm (**PTCDI-P**).

Table 3. Stokes shift of title compounds calculated with λ_{em} and λ_{abs}.

	λ_{em} (nm)	λ_{abs} (nm)	Stokes shift (nm)
BTD-P	495	445	50
NDI-P-1	583	514	69
NDI-P-2	586	514	72
PTCDI-P	611	587	24

Comparing the title compounds in Figure 5 shows that λ_{em} is significantly red-shifted from **BTD-P** to **NDI-P-1**/**NDI-P-2**, then a less dramatic red-shift for **PTCDI-P**. This is a

different trend compared to the gradual shift seen with UV-Vis. Listed in Table 3, is λ_{em} of the title compound's along with the calculated Stokes shift. **PTCDI-P** shows the longest λ_{em} of 611 nm, with the smallest Stokes shift of 24 nm. **NDI-P-1** and **NDI-P-2** show λ_{em} of 583 nm and 586 nm, with a Stokes shift of 69 nm and 72 nm respectively. Additionally, **BTD-P** shows λ_{em} of 495 nm, with a Stokes shift of 50 nm.

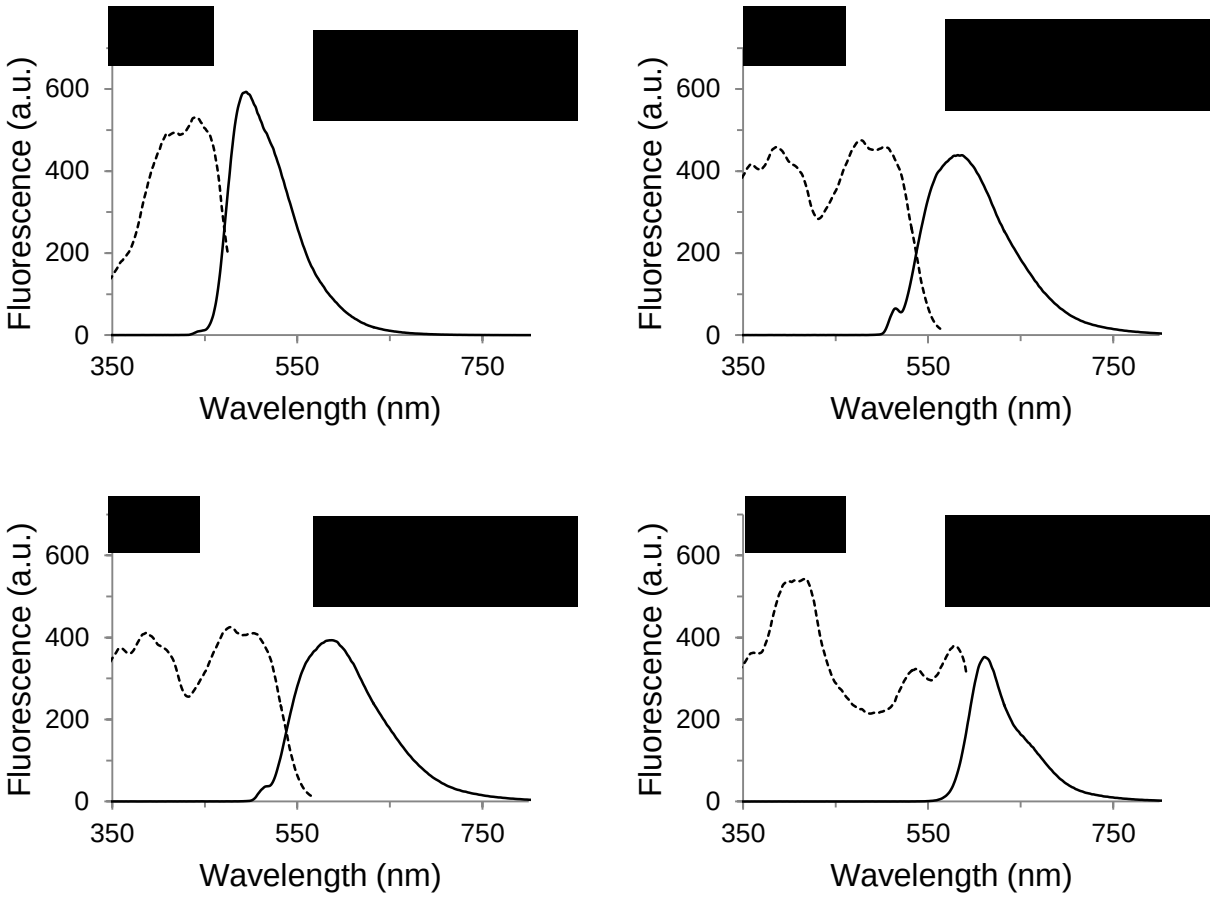

Figure 6. Fluorescence emission (solid line) and excitation (dotted line) spectra of **BTD-P** (a), **NDI-P-1** (b), **NDI-P-2** (c), and **PTCDI-P** (d) in dichloromethane solution.

The excitation spectra of **BTD-P**, **NDI-P-1**, **NDI-P-2**, and **PTCDI-P** in dichloromethane were collected at λ_{obsd} = 495, 583, 586, and 611 nm, respectively. The resulting excitation spectra is plotted against fluorescence emission and shown in Figure 6. To obtain the excitation spectra,

λ_{obsd} was set to their respective λ_{em} so that only the fluorophore which emits at λ_{em} can be excited. Note here that the recorded excitation spectra for the title compounds matches their UV-Vis absorption spectra.

Additional fluorescence emission was studied for **BTD-P**, **NDI-P-1**, **NDI-P-2**, and **PTCDI-P** in the solid state. However, the emission of **PTCDI-P** in the solid state was not strong enough for accurate detection. Therefore, the solid state emission spectra in Figure 7 only shows those of **BTD-P**, **NDI-P-1** and **NDI-P-2**. The samples used for solid state analysis were prepared as a cast film from dichloromethane solution at a 5 μM concentration.

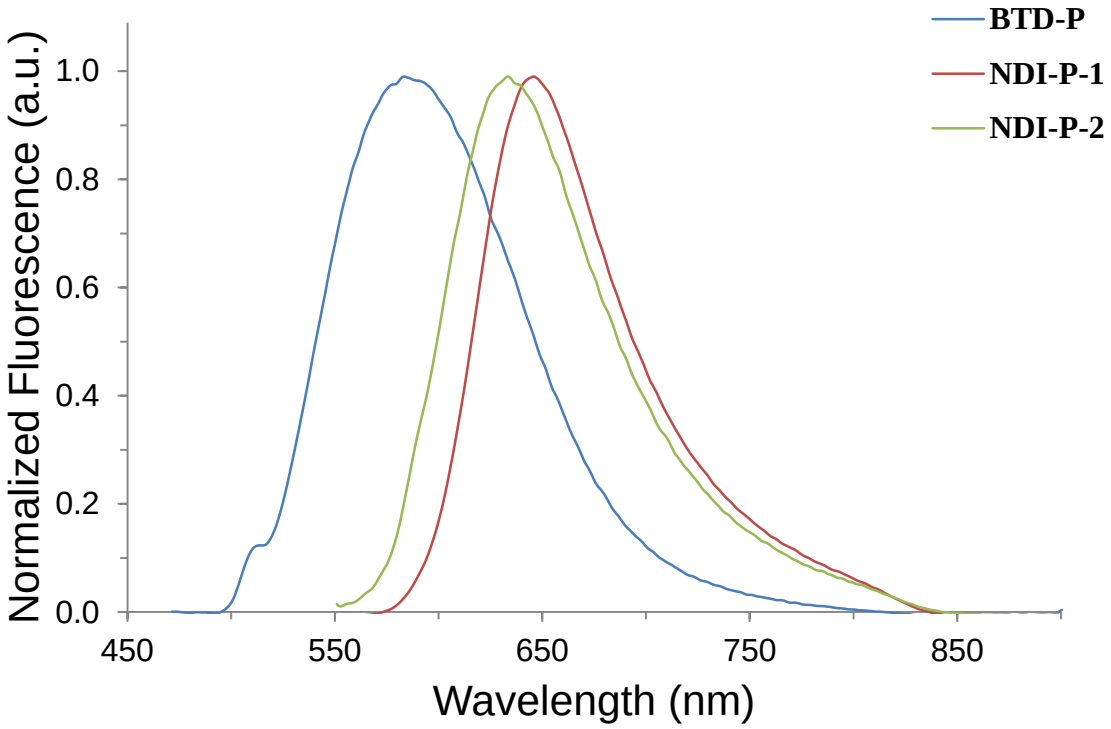

Figure 7. Normalized emission spectra for **BTD-P**, **NDI-P-1** and **NDI-P-2** in solid state, excited at 453 nm, 536 nm, and 535 nm respectively.

The solid state emission spectra of **BTD-P**, **NDI-P-1** and **NDI-P-2** are displayed in Figure 7. For **BTD-P**, λ_{em} in the solid state is seen at 580 nm. For **NDI-P-1**, λ_{em} is red-shifted to

641 nm. For **NDI-P-2**, λ_{em} is seen at 628 nm. The solid state emission spectra seen for these compounds can also be compared to their solution spectra. When compared, a similar pattern is seen with that of the UV-Vis absorption spectra for solid and solution state. Similar to the absorption, all compounds experienced red-shifted emission in the solid state compared to their solution state. **BTD-P** gave the most extensive shift of 85 nm with λ_{em} = 495 nm in solution and λ_{em} = 580 nm in the solid state. The next significant shift of 58 nm was seen for **NDI-P-1** with λ_{em} = 583 nm in solution and λ_{em} = 641 nm in the solid state. Lastly, **NDI-P-2** showed a red-shift of 42 nm with λ_{em} = 586 nm in solution and λ_{em} = 628 nm in the solid state. Rationale for the red-shifted emission in the solid state is the same as what was described for UV-Vis absorption spectroscopy. The *J*-aggregates seen by the solid phase samples strongly supports intermolecular π-π interactions.[43] Presumably, **NDI-P-1** in the solid-state is more red-shifted than **NDI-P-2** because of the molecular packing differences caused by a bulky versus straight chain. This would only cause spectral differences in the solid-state while the solution fluorescence spectra remains the same.

3.3 Electrochemical Properties

The effect on electrochemical properties by changing the electron deficiency of the pendant on the title molecules was examined using cyclic voltammetry. The compounds were tested in a dichloromethane solution with $TBAPF_6$ (0.1 M) as the supporting electrolyte, $Ag/AgNO_3$ in CH_3CN as the reference electrode solution, and Ferrocene as an internal reference. The resulting cyclic voltammograms are shown in Figure 8.

3.3.1 Cyclic Voltammetry

Measuring the redox potentials will determine the amount of energy required to gain or lose and electron, and thus the HOMO/LUMO energy levels for the title compounds can be

calculated from oxidation and reduction potentials.[44] The potential for the first reduction peak represents the energy required to gain an electron and can be directly related to the LUMO energy level (E_{LUMO}) of a compound, which is our primary focus. Therefore, the onset of the first reduction peak was measured to calculate E_{LUMO} for all title compounds, using ferrocene's oxidation potential of -4.8 eV with respect to vacuum.[45]

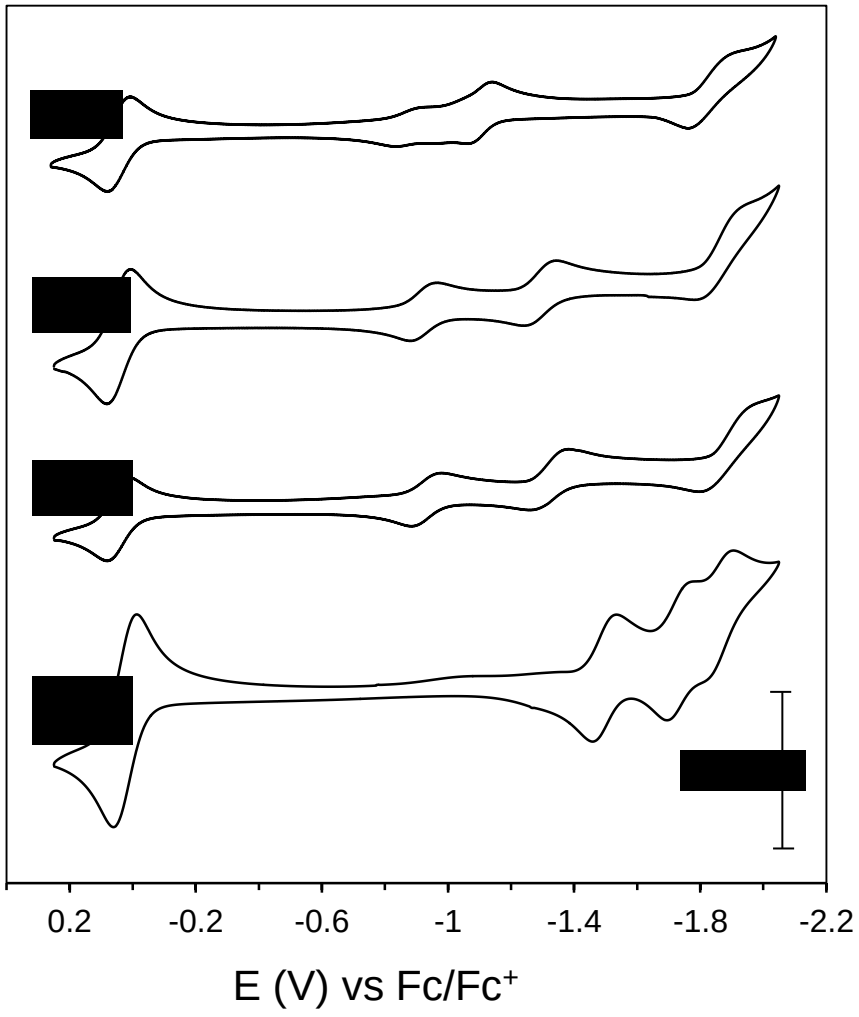

Figure 8. Cyclic voltammograms for the reduction of **PTCDI-P** (a), **NDI-P-2** (b), **NDI-P-1** (c), **BTD-P** (d). Scan rate: 100 mV/s

Shown in Figure 8, are the cyclic voltammograms obtained for title compounds **BTD-P**, **NDI-P-1**, **NDI-P-2**, and **PTCDI-P**. It can be seen that the onset of the first reduction peak decreases in energy as the pendant of the title molecules becomes more electron deficient. The electron withdrawing power of the pendant for the title compounds is increasing in the order of **BTD-P**, **NDI-P-1**/**NDI-P-2**, to **PTCDI-P**. Accordingly, **BTD-P** gave the highest E_{LUMO} of -3.34 eV. The trend continues with **NDI-P-1**/**NDI-P-2** showing a significantly more stabilized E_{LUMO} of -3.90 eV. The lowest E_{LUMO} is seen from **PTCDI-P** at -3.97 eV, however only slightly lowered from those of **NDI-P-1** and **NDI-P-2**. These values are displayed in Table 4. In correlation with UV-Vis spectroscopy which showed the same order of E_{gap}^{opt} compression, it can be deduced that lowering E_{LUMO} is the major contribution to the reduction of E_{gap}.

Table 4. Calculated E_{LUMO} levels for title compounds using Cyclic Voltammetry

	E_{red}^{onset} **(eV)**	E_{LUMO} **(eV)**
BTD-P	-1.46	-3.34
NDI-P-1	-0.90	-3.90
NDI-P-2	-0.90	-3.90
PTCDI-P	-0.83	-3.97

3.4 Theoretical Evaluation

3.4.1 HOMO and LUMO Energy Levels

To examine our experimental data in comparison to theoretical results, a computational investigation of the electronic properties was carried out for the title molecules. Initially, geometries were optimized at the B3LYP/6-31G* level of theory. Results from these calculations are presented in Table 5.

Table 5. Summary of electronic properties

	E_{LUMO}^{EXP} [a] [eV]	E_{HOMO}^{EXP} [b] [eV]	E_{gap}^{EXP} [c] [eV]	E_{LUMO}^{THEO} [d] [eV]	E_{HOMO}^{THEO} [d] [eV]	E_{gap}^{THEO} [e] [eV]
BTD-P	-3.34	-5.87	2.51	-2.75	-5.30	2.55
NDI-P-1	-3.90	-6.13	2.23	-3.29	-5.61	2.32
NDI-P-2	-3.90	-6.13	2.23	-3.29	-5.61	2.32
PTCDI-P	-3.97	-5.94	1.97	-3.37	-5.48	2.11

[a] from cyclic voltammetry [b] $E_{HOMO}^{EXP} = E_{LUMO}^{EXP} - E_{gap}^{EXP}$ [c] from UV-Vis
[d] calculated using B3LYP/6-31G* [e] $E_{gap}^{THEO} = E_{LUMO}^{THEO} - E_{HOMO}^{THEO}$

The experimental E_{HOMO}, was calculated by subtracting E_{gap}^{opt} from E_{LUMO} obtained from cyclic voltammetry. Using the values in Table 5, a direct comparison can be made between experimental and theoretical energy levels. A graphical representation of this comparison is displayed in Figure 9.

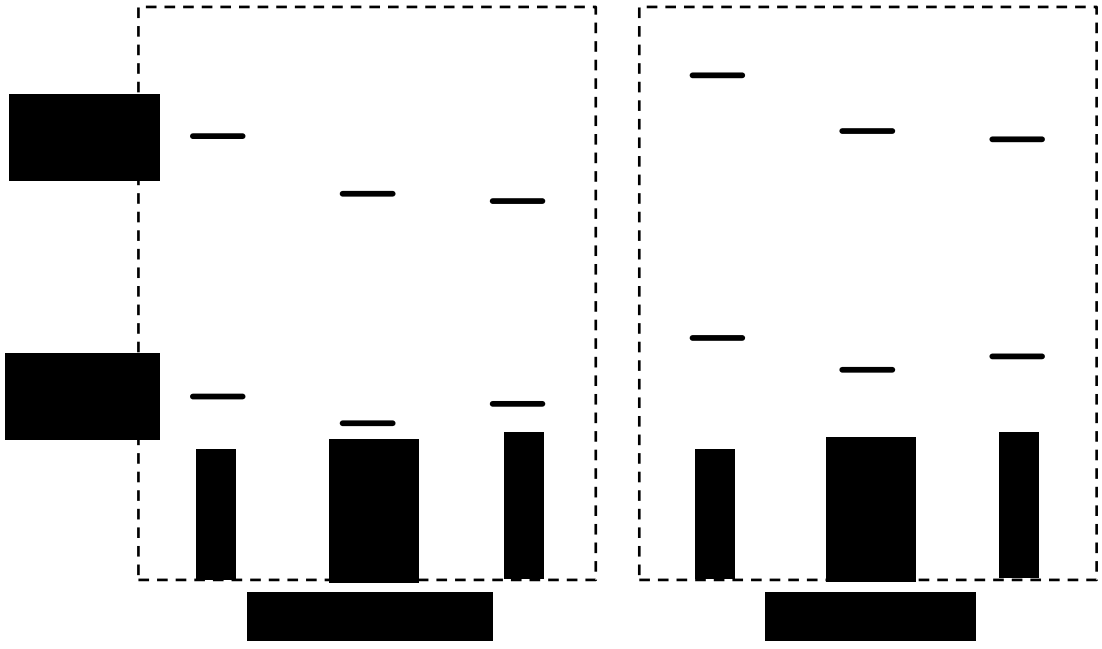

Figure 9. Graphical representation of electronic properties.
Numerical values are provided in Table 5.

When comparing the experimental and theoretical HOMO and LUMO energies of the title compounds in Figure 9, a similar trend can easily be seen. For both theoretical and experimental values, E_{LUMO} decreases in the order **BTD-P**, **NDI-P-1**/**NDI-P-2**, **PTCDI-P**. Additionally, both results show E_{HOMO} decreasing from **BTD-P** to **NDI-P-1**/**NDI-P-2** and then increasing for **PTCDI-P**. The increase in E_{HOMO} for **PTCDI-P** is likely a result of HOMO orbital localization and is explained in more detail in the following section. Also shown in Figure 9, a similarity in E_{gap} between experimental and theoretical results is observed. The E_{gap} calculated theoretically is nearly identical to the experimental E_{gap}, with a difference of only about 0.10 eV. With such matching trends, theoretical evaluation serves as a crucial tool in our research for not only understanding, but predicting purposes as well.

3.4.2 Frontier Molecular Orbital Diagrams

Additional theoretical calculations can be used to predict how the frontier molecular orbitals (FMOs) are distributed over the title molecules. This study allows us to visually inspect whether the electronic property of the pendant affects both E_{LUMO} and E_{HOMO} simultaneously or one of them more significantly. The FMOs for the title compounds **BTD-P**, **NDI-P-1**, **NDI-P-2**, and **PTCDI-P** are presented in Figure 10. We note that the different alkyl chains on **NDI-P-1** and **NDI-P-2** have no effect on the HOMO and LUMO orbitals and are therefore combined as one FMO diagram. For all compounds, the LUMO orbitals are localized on the pendant of the molecule and thus electron-deficiency of the pendant was reflected in E_{LUMO}. Meanwhile, HOMO orbitals are distributed over the molecules including phenazines. However, they exclude the most electron-withdrawing thiadiazole (for BTD) and imide (for NDI and PTCDI). Therefore, the electron-deficiency of the pendant was less translated to E_{HOMO}. Of particular interest is the higher E_{HOMO} of **PTCDI-P** compared to that of **NDI-P-1/NDI-P-2**. Presumably, it

is due to the inclusion of electron-deficient imine nitrogen in phenazine of **NDI-P-1**/**NDI-P-2** while negligible distribution of HOMO orbital was on the imine nitrogen of **PTCDI-P**. These molecular orbital pictures are essential in gaining understanding into how the changes in electron deficiency of the pendant affect the electronic properties of the title molecules.

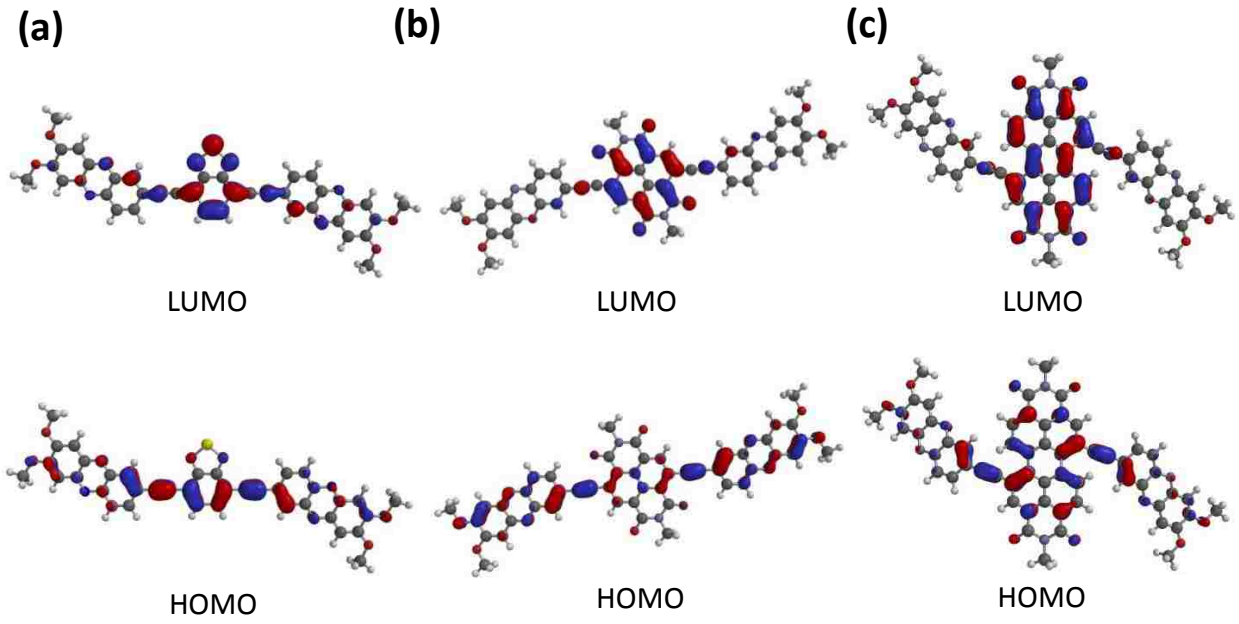

Figure 10. Molecular orbital diagrams of title compounds:
(a) **BTD-P**; (b**) NDI-P-1** and **NDI-P-2**; and (c) **PTCDI-P**.

3.4.3 Energy Minimized Structures-Dihedral Angles

The energy minimized structures of the title compounds are shown in Figure 11. It can be seen that the structures for both **BTD-P** and **NDI-P-1**/**NDI-P-2** show planar geometry. However, **PTCDI-P** shows a "puckered" conformation. With their planar structure, **BTD-P**, **NDI-P-1** and **NDI-P-2** all have a dihedral angle of 0^{o} between A-A'-A, while **PTCDI-P** has a dihedral angle of 17.20^{o}.

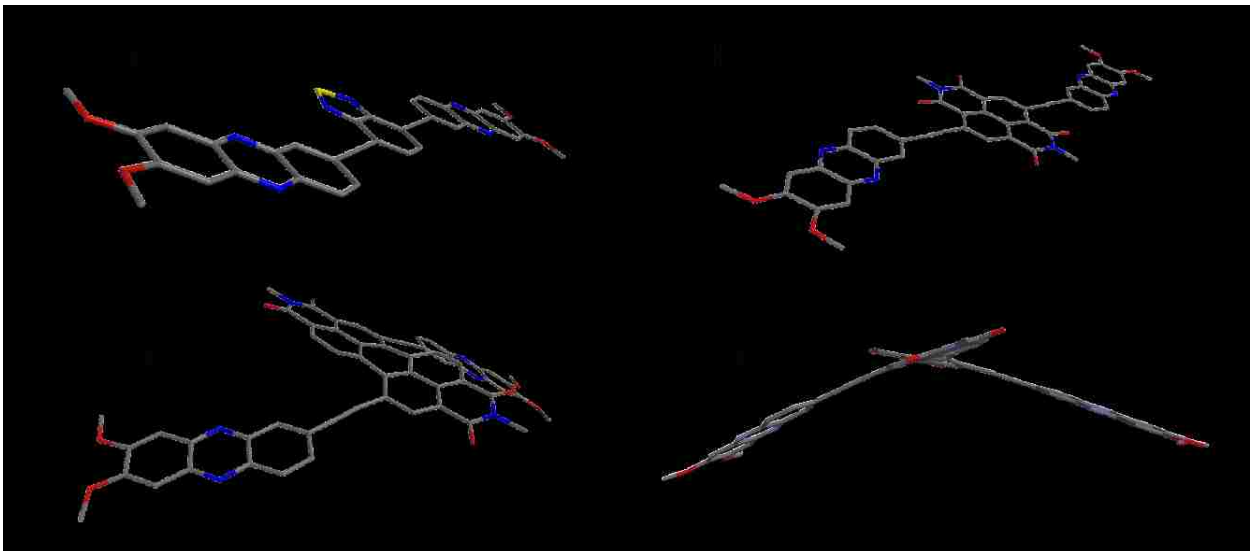

Figure 11. Energy minimized structures of **(a) BTD-P**, dihedral angle = 0^{o}; **(b) NDI-P-1** and **NDI-P-2**, dihedral angle = 0^{o}; **(c) PTCDI-P**, dihedral angle = 17.20^{o} **(d)** alternate view of (c)

3.5 Thermal Properties

3.5.2 Differential Scanning Calorimetry

The thermal phase transitions of **BTD-P**, **NDI-P-1**, **NDI-P-2** and **PTCDI-P** were studied by differential scanning calorimetry (DSC). Of the four title compounds, **BTD-P** was the only compound that showed reversible phase transitions over two heating/cooling scans (Figure 12).

The first heating cycle ran on **BTD-P** showed a melting endotherm (T_m) at 175^{o}C with a heat of melting of 47.09 J/g. The first cooling cycle showed a recrystallization exotherm (T_c) at 171^{o}C. Correspondingly, there was a T_m at 178^{o}C with a heat of melting of 45.65 J/g in the second heating cycle, and the second cooling cycle showed a T_c at 171^{o}C. **BTD-P** was the only title compound that showed melt stability. A low temperature endotherm at the first heating cycle (163 ^{o}C) appeared to be due to a pre-existing nonintrinsic molecular arrangement as it is not reproducible at the second heating scan.

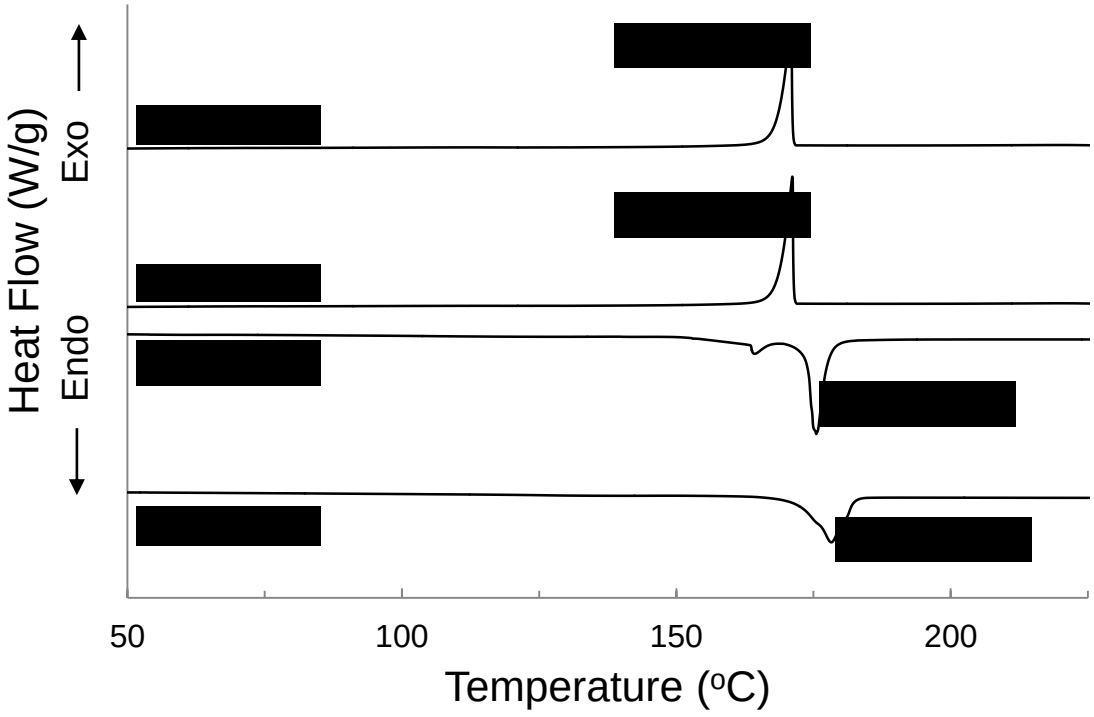

Figure 12. DSC thermograms of **BTD-P** obtained at heating and cooling rates of 10 °C/min in nitrogen.

The DSC thermograms in Figure 13 show T_m for **NDI-P-1**, **NDI-P-2** and **PTCDI-P**. **NDI-P-1** showed a T_m at 254°C with a heat of melting of 25.73 J/g. **NDI-P-2** showed a T_m at 222°C with a heat of melting of 33.54 J/g. **PTCDI-P** showed a T_m at 192°C with a heat of melting of 29.92 J/g. As previously noted, T_c could not be obtained for these compounds, nor could a second heating/cooling cycle. This was due to the additional exotherm peak positioned shortly after T_m for all three compounds. This exotherm is likely a result of a possible cyclization reaction occurring between the triple bonds and the aromatic rings for **PTCDI-P**[48] or between carbonyl in the pendant for **NDI-P-1** and **NDI-P-2**.[46-47] This cyclization reaction has been seen in previous research as a core-expansion of perylenediimide including annulation of benzene rings and heterocycles of the perylene core.[48]

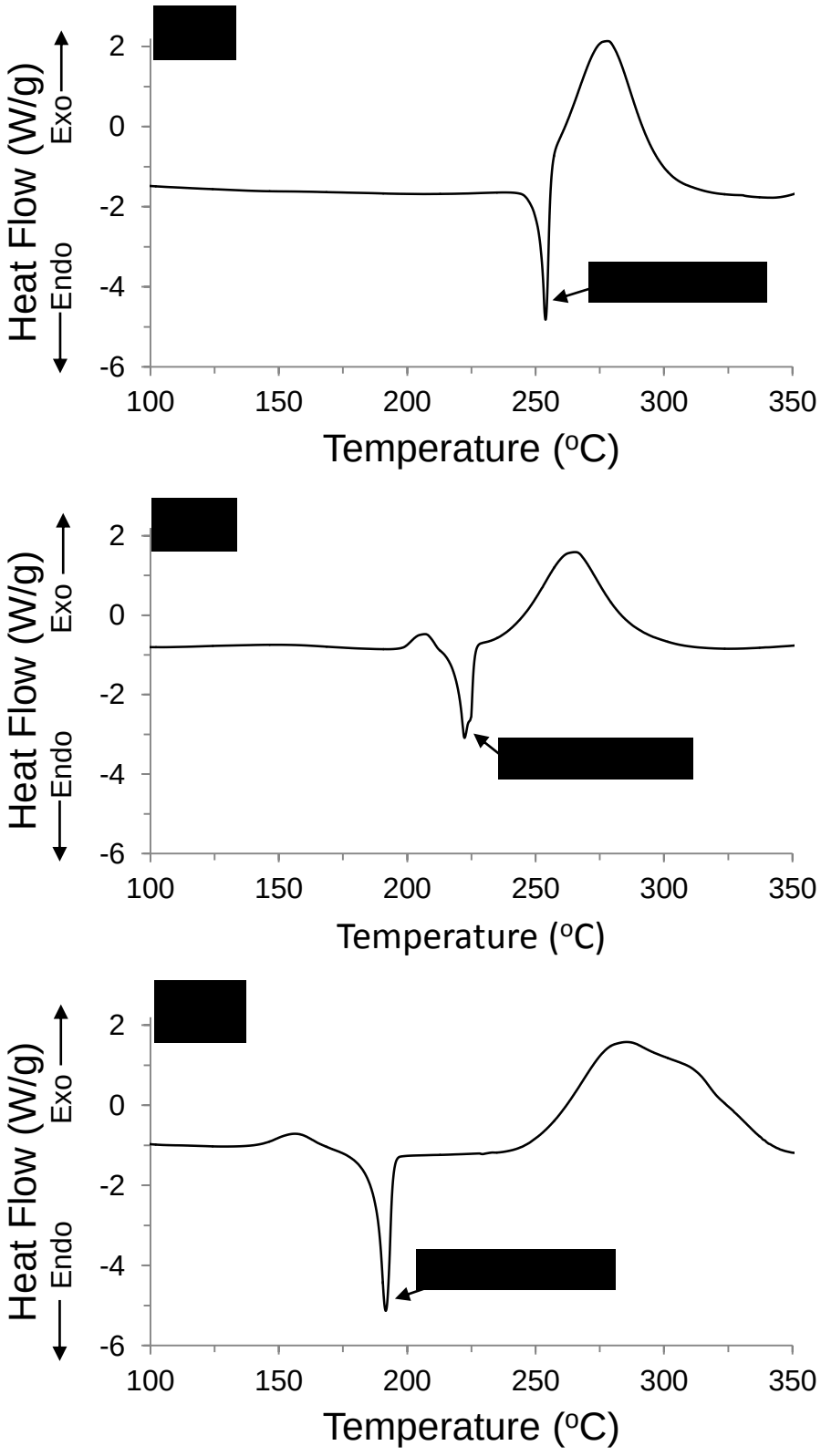

Figure 13. DSC thermograms of **NDI-P-1** (a); **NDI-P-2** (b); and **PTCDI-P** (c); obtained at heating and cooling rates of 10°C/min in nitrogen.

We initially expected that the bulkier alkyl group in the molecular structure of **NDI-P-1** would reduce the π-π interaction. However, shorter alkyl group in **NDI-P-1** could be related to the higher melting point seen for this compound. The lower solubility of **NDI-P-1** compared to **NDI-P-2** as explained in section 3.1 also supports the trend in melting temperature. Although **NDI-P-1** showed a higher T_m than **NDI-P-2**, it should be noted that the straight octyloxy group of **NDI-P-2** facilitates better molecular packing and thus crystallization revealed by the heat of fusion.

In addition, the low T_m of **PTCDI-P** was quite unexpected. We presumed that **PTCDI-P** would possess the highest T_m due to its larger π-surface. This result can be best explained with molecular geometry from theoretical calculations described in section 3.4. In Figure 11 of section 3.4, we see that **PTCDI-P** adapts non-planar geometry and especially, **PTCDI-P** is puckered with a fold angle of 17.20^o. Due to the non-planarity, intermolecular interactions would be limited and could explain why the T_m for **PTCDI-P** was so low.

4 CHARGE TRANSFER

To test the title compounds as potential charge transfer (CT) acceptors (A), they must be paired with a donor (D) that has appropriate electronic porperties.[49] Appropriate donor should possess low ionization potential (high E_{HOMO}). Additionaly, planarity of the donor helps promote π-stacking of D and A, which is typical for CT complexes.[49-50] Based on this criteria, pyrene was chosen as a donor to test the CT ability with the title molecules. Pyrene is a common CT donor, having a planar structure and low ionization potential with theoretical E_{HOMO} = -5.21 eV[51] and E_{LUMO} = -1.38 eV[51] (calculated using B3LYP/6-31G*).

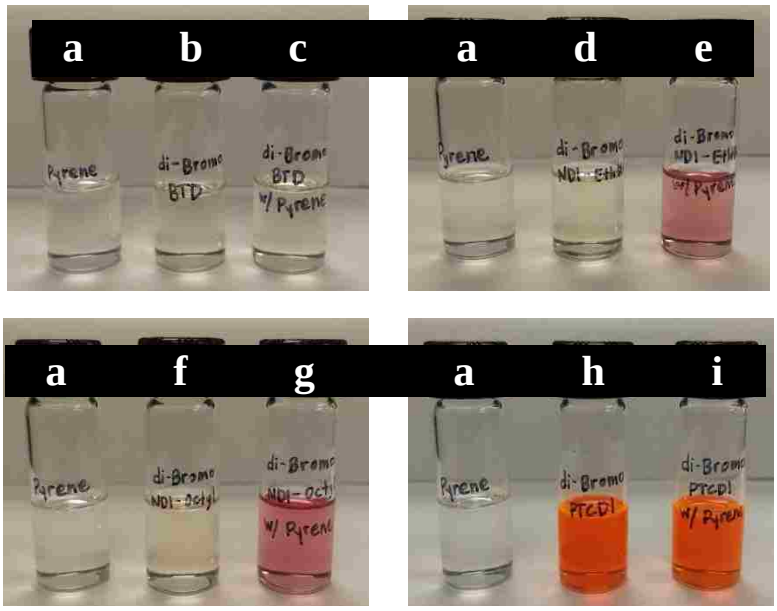

Figure 14. 5mM CH_2Cl_2 solutions of **(a)** pyrene; **(b)** diBr-BTD; **(c)** equimolar mixture of (a) and (b); **(d)** diBr-NDI-1; **(e)** equimolar mixture of (a) and (d); **(f)** diBr-NDI-2; **(g)** equimolar mixture of (a) and (f); **(h)** diBr-PTCDI; (**i**) equimolar mixture of (a) and (h).

An early experiment identifying CT can be made from the color changes as shown in Figure 14. These color changes are indicative of the formation of a CT band.[52] The CT band may form by hybridizing the HOMO level of the donor and the LUMO level of the acceptor.[53] As a preliminary experiment, 5 mM chloroform solutions of the CT donor (pyrene) and acceptor (dibromo-pendant) were made. The solution color was observed individually and compared to the solution color of donor:acceptor mixture at 1:1 ratio. As seen from Figure 14, the chloroform solution of CT donor (pyrene) is colorless. The chloroform solutions of CT acceptors, 4,7-dibromo-2,1,3-benzothiadiazole (**9**), di-(2-ethyl-1-hexyl)-2,6-dibromo1,4,5,8-napthalenetetracarboxylic acid bisimide (**15**), and dioctyl2,6-dibromo1,4,5,8-napthalenetetracarboxylic acid bisimide (**16**) are also colorless, and di-(2-ethyl-1-hexyl)-1,7-dibromo3,4:9,10-perylenetetracarboxylic acid bisimide (**21**) is a bright orange. Note that the CT acceptors are primarily the pendant, the most electron-deficient part of the title molecules. When

the two solutions were mixed at a 1:1 ratio of 5 mM:5 mM, the only color change observed is when the CT acceptor was NDI (Figure 14 e and g), resulting in a red solution. This color change is a result of CT band formation. Presumably, the electron-deficiency of BTD is not high enough to induce CT with pyrene. Additionally, lack of color change with PTCDI could be related to a non-planar structure.

4.1 Optical Properties

4.1.1 UV-Vis Absorption Spectroscopy

With this initial CT experiment in solution in mind, we prepared films of **NDI-P-1** and **NDI-P-2** with and without pyrene to assess CT in the solid-state. To fabricate the cast films without pyrene, 5 mM solutions of **NDI-P-1** and **NDI-P-2** in 1,1,1-trichloroethane (TCE) were prepared. For the films with pyrene, mixture solutions were prepared by mixing a 1:1 ratio of 10 mM pyrene in TCE with 10 mM **NDI-P-1** or **NDI-P-2** in TCE. The solutions were then spread onto a glass slide using a pipette and the solvent was allowed to evaporate. Using the prepared cast films, CT properties of pyrene/**NDI-P-1**, and pyrene/**NDI-P-2** were studied using UV-Vis spectroscopy. The absorption spectra for the films without pyrene are compared to the films with pyrene and are displayed in Figure 15.

If there was any CT occurring between the pyrene donor and the title compounds, a red-shift to longer wavelength with tailing would be observed. This red-shift is correlated to a smaller E_{gap} of the CT complex compared to the E_{gap} of the original donor and acceptor molecules. When comparing the absorption spectra from Figure 15, a larger red-shift of 38 nm is seen with **NDI-P-1** compared to 29 nm with **NDI-P-2**. Additionally, both spectra show pyrene absorption as seen from the peak near 350 nm. Even though the red-shift is likely related to CT,

it could also be a result of changed molecular packing due to the presence of pyrene. To further investigate CT interaction, fluorescence spectroscopy was conducted.

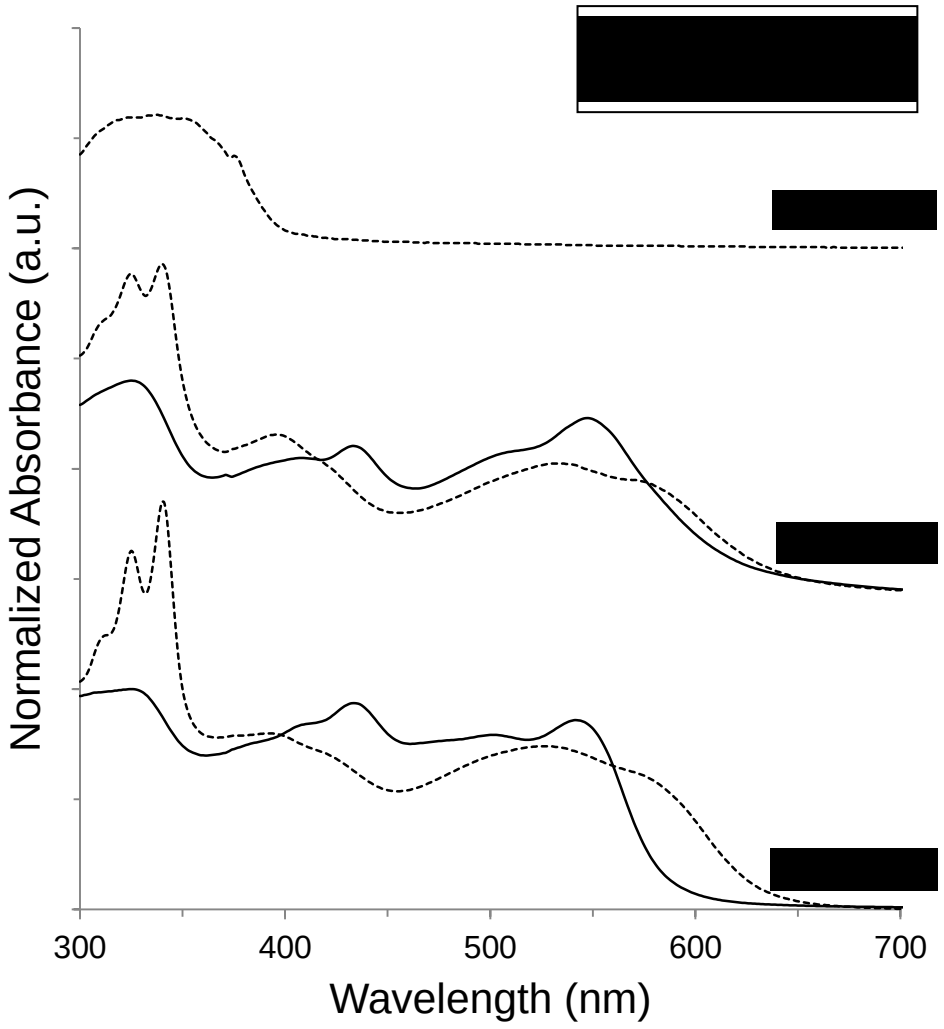

Figure 15. UV-Visible absorption spectra for **NDI-P-1** and **NDI-P-2**as a 5mM TCE cast film with (dotted line) and without (solid line) pyrene. UV-Visible absorption spectrum for 5mM TCE cast film of pyrene (dotted line) shown for comparison.

4.1.2 Fluorescence Spectroscopy

Fluorescence spectroscopy was employed to characterize pyrene/**NDI-P-1** and pyrene/**NDI-P-2** using the same films that were used for UV-Vis characterization. The resulting

emission spectra for the films without pyrene are compared to the films with pyrene and are displayed in Figure 16.

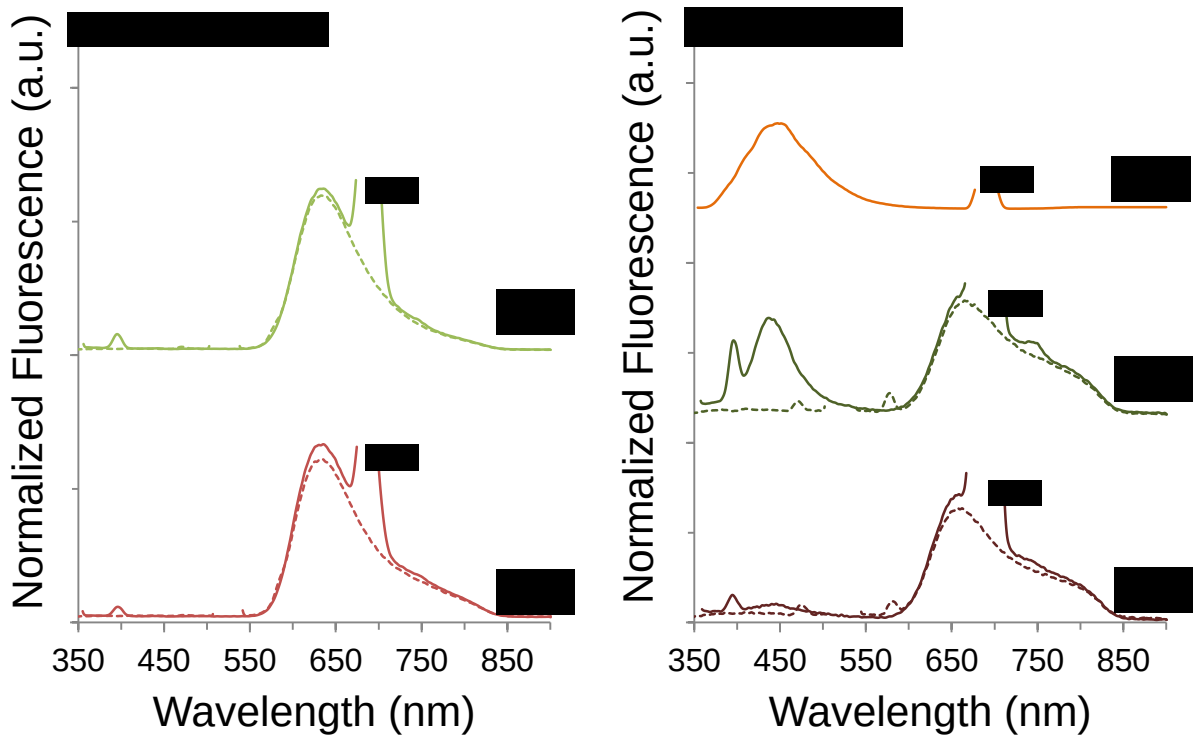

Figure 16. Fluorescence spectra of **(a) NDI-P-1**, λ_{exc} = 528nm (broken line) λ_{exc} = 340nm (solid line), **(b) NDI-P-2**, λ_{exc} = 523nm (broken line) λ_{exc} = 340nm (solid line), **(c)** pyrene/**NDI-P-1**, λ_{exc} = 528nm (broken line) λ_{exc} = 340nm (solid line), **(d)** pyrene/**NDI-P-2**, λ_{exc} = 523nm (broken line) λ_{exc} = 340nm (solid line); and **(e)** pyrene, λ_{exc} = 340nm (solid line). All films were casted from 5mM TCE solution. *2nd order diffraction peak

The fluorescence spectra for **NDI-P-1** and **NDI-P-2** with and without pyrene are displayed in Figure 16. Additionally, Figure 16 shows the fluorescence spectra for pyrene only as a comparison. It can be seen that emission around 450 nm occurs when pyrene is excited at 340 nm. Therefore, to test CT with pyrene/**NDI-P-1** and pyrene/**NDI-P-2**, the samples were also excited at 340 nm. If CT occurred, excitation at 340 nm should not show any pyrene emission because the electron from pyrene's LUMO has transferred to the LUMO of the acceptor. This

quenching of pyrene's emission is seen for pyrene/**NDI-P-1**, however pyrene/**NDI-P-2** showed residual fluorescence of the donor. Note that the emission spectra for both pyrene/**NDI-P-1** and pyrene/**NDI-P-2** show a long wavelength shoulder compared to the fluorescence spectra without pyrene. This long wavelength shoulder is probably due to the new band formation seen with a CT complex. Although both CT systems show the long wavelength shoulder, only pyrene/**NDI-P-1** shows almost complete quenching of pyrene's emission. As a way to test the emission seen near 425 nm is in fact from pyrene and not from the title molecules, the emission spectra for **NDI-P-1** and **NDI-P-2** without pyrene were tested at the same excitation wavelengths. Seen from their spectra in Figure 16, no emission is observed when excited at 340 nm for either of the two **NDI-P** molecules.

Given the FL spectra differences between pyrene/**NDI-P-2** and pyrene/**NDI-P-2**, it can be concluded that CT is more efficient using **NDI-P-1** as an acceptor. Presumably, the bulky alkyl chain of **NDI-P-1** facilitates more room between molecules so that pyrene can intercalate more efficiently. However, the straight alkyl chain in **NDI-P-2** could induce a tighter molecular packing which would not allow pyrene to be incorporated. To test this hypothesis, the assembly properties were studied using polarized optical microscopy (POM).

4.2 Assembly Properties

4.2.1 Polarized Optical Microscopy

Our primary goal is to investigate if fibers of CT complex can be made. Since the title compounds were designed for 1D assembly, we examined their fibrillation capability using POM. The morphology was studied from the same films characterized for UV-Vis and fluorescence spectroscopy. The POM images from the films without pyrene are displayed in Figure 17 as (a) and (d) for **NDI-P-1** and **NDI-P-2**, respectively. Additionally, the POM image

for pyrene/**NDI-P-1** is displayed in Figure 17 as (b) and under cross-polarization as (c); while pyrene/**NDI-P-2** is displayed as (e) and under cross-polarization as (f).

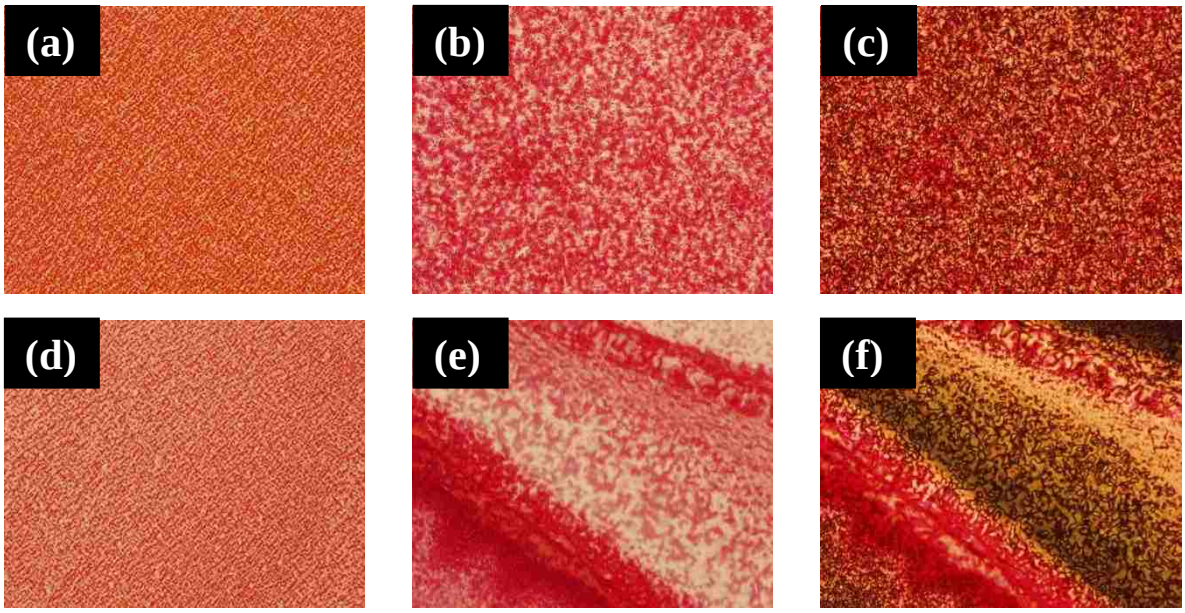

Figure 17. POM images of **(a) NDI-P-1**, **(b)** pyrene:**NDI-P-1** (1:1), **(c)** x-polarization of (b), **(d) NDI-P-2**, **(e)** pyrene:**NDI-P-2** (1:1), **(f)** cross-polarization of (e), as cast films from TCE solution. Image width: 110 μm

A comparison can be made from the images in Figure 17 of the morphology changes when pyrene was added to **NDI-P-1** versus **NDI-P-2**. For **NDI-P-1** with pyrene, the film from image (b) and (c) shows homogeneous distribution throughout the film which suggests that pyrene may have been incorporated into the structure. It should be noted that clear fiber structures were observed at the thinner area of the film. However, the **NDI-P-2** film with pyrene from image (e) and (f) show clear phase separation of the two molecules.

5 ENERGY TRANSFER THROUGH ORGANOGELATION

Fluorescence resonance energy transfer (FRET) occurs when the emission of a donor (D) is absorbed by an acceptor (A). In simpler terms, the donor's energy is transferred to the acceptor. Efficiency of FRET is highly dependent on the distance between the D and A molecules.[24,54] To ensure high FRET efficiency, two component fibers of D and A is beneficial for better distance control. In that regard, organogelation[55] is an efficient method to create fibers. Since the title compounds were designed for 1D self-assembly, their organogelation properties were investigated first. Then, the formation of two component gel was tested for FRET.

5.1 Organogelation

Organogelation was studied for **BTD-P**, **NDI-P-1** and **NDI-P-2** using select organic solvents.[56-58] Typically, the compounds were suspended in TCE at known concentrations and then heated until they were fully dissolved. The solutions were then left undisturbed as they cooled to room temperature and observed for the formation of a gel. When turning the vial upside down, successful gelation was identified if there was no streaming solvent.[39] The lack of flow is created as the solvent becomes trapped in a 3D network of 1D fibers. In this sense, organogelation is a good indicator of fiber formation and is useful to determine self-assembling ability.[59-60] All compounds were tested at concentrations of 3 mM, 5 mM and 10 mM in TCE, and their results are summarized in Table 6. The only compound with successful gel formation was **BTD-P**. Both **NDI-P-1** and **NDI-P-2** formed a precipitate upon cooling. This precipitation was studied under POM, which showed short fibers. We assume that the length of fibers is too short for gelation.

Table 6. Gelation test of **BTD-P**, **NDI-P-1** and **NDI-P-2** in TCE

Concentration	BTD-P	NDI-P-1	NDI-P-2
3 mM	PG	ppt	ppt
5 mM	G	ppt	ppt
10 mM	G	ppt	ppt

[a]Abbreviations: G, gel; PG, partial gel; ppt, precipitation upon cooling

The fact that **BTD-P** gelled TCE was advantageous for FRET since **BTD-P** and **NDI-P-2** meet the spectral requirement for donor and acceptor, respectively. Therefore, organogelation for D/A mixture was conducted with **BTD-P** as a donor and **NDI-P-2** as an acceptor with acceptor concentrations of 5 mole% and 10 mole%. For both ratios, the concentration of **BTD-P** in TCE was kept to 5 mM. As **NDI-P-2** did not show gelation ability in TCE, our major concern was if the gel of **BTD-P** could be maintained. At both acceptor concentrations, gel formation was successful. It was encouraging that the nongelator **NDI-P-2** did not disrupt the gelation of **BTD-P**. The pictures of **BTD-P** gel and mixture gel of **BTD-P** and 10 mole% **NDI-P-2** are shown in Figure 18. This figure shows a significant color change from a bright orange for **BTD-P** to a dark red even with only 10 mole% of **NDI-P-2**. Under the illumination at 365 nm, **BTD-P** gel showed strong yellow emission, while the **BTD-P** with 10 mole% **NDI-P-2** gel showed the red emission with lower intensity. This suggests an efficient FRET since the donor's emission would be absorbed by the acceptor and only emission of the acceptor should be seen.

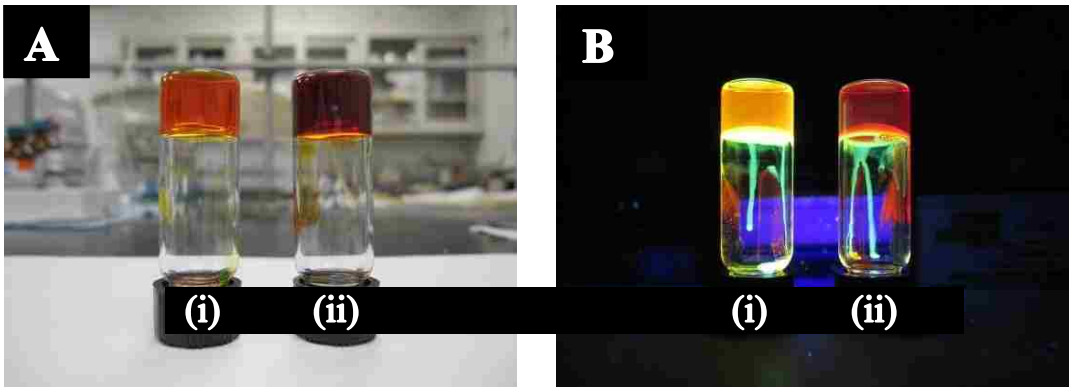

Figure 18. Picture of **BTD-P** gel (i) and **BTD-P** with 10mole% **NDI-P-2** (ii) in TCE. Image A is under room light and image B is under illumination at 365 nm.

5.1.1 Polarized Optical Microscopy

To further study morphology of gels, dried gels were prepared and studied using POM. Figure 19 **A** shows the long fibers formed from the **BTD-P** xerogel, with a bright orange/yellow color. For the **BTD-P** with 10 mole% **NDI-P-2** xerogel shown in Figure 19 **B**, homogeneous distribution is seen and the color has changed to more of a red. Fiber formation is also observed in image **B**, but using POM is insufficient to determine if **NDI-P-2** has been incorporated into the fiber or remained in solution. Nevertheless, it is promising that no discernible phase separation was observed. Further study with high-power microscopy such as field-emission scanning electron microscopy or transmission electron microscopy would be necessary to determine if a two component fiber was formed.

Figure 19. POM images of (A) BTD-P xerogel and (B) BTD-P with 10 mole% NDI-P-2 xerogel. Both xerogels were prepared from TCE gels. Image width: 110 μm

5.2 Optical Properties

The emission spectra for **BTD-P** in solution showed λ_{em} = 495 nm and **NDI-P-2** λ_{em} = 586 nm. The absorption spectra for **BTD-P** in solution showed λ_{max} = 445 nm and **NDI-P-2** λ_{max} = 514 nm. For efficient FRET, you need the emission spectrum of the donor to overlap with the absorption spectrum of the acceptor. Since emission wavelength of **BTD-P** (495 nm) is not much different than the absorption of **NDI-P-2** (514 nm), FRET was tested using **BTD-P** as the donor and **NDI-P-2** as the acceptor as a two component gel. This system was studied using fluorescence emission spectroscopy.

5.2.1 Fluorescence Spectroscopy

To determine FRET, we would expect to observe acceptor emission using indirect excitation of the donor. When the donor is excited, its emission is absorbed by the acceptor so that only acceptor emission will be seen if FRET is successful. To test this concept, we first determined the correct λ_{exc} from excitation spectra with λ_{obsrd} at their λ_{em}. For **BTD-P** gel, λ_{exc} was found to be 500 nm, while that for **BTD-P**/**NDI-P-2** gel was 570 nm. When the donor (5 mM **BTD-P** gel) was excited using direct excitation at 500 nm, λ_{em} was 553 nm. We then tested the emission spectra for both 5% and 10% acceptor concentrations of the donor/acceptor (**BTD-**

P/NDI-P-2) gel when excited at the same wavelength. If no FRET had occurred, excitation at 500 nm would produce **BTD-P**'s emission at 553 nm. If FRET was successful, we would expect **NDI-P-2**'s emission only at 651 nm. Note that excitation of **NDI-P-2** without **BTD-P** at 500 nm does not show any significant emission. Shown in Figure 20, **BTD-P**'s fluorescence was completely disappeared and only the emission at λ_{em} = 651 nm was observed, which is indicative of FRET. More interestingly, the same level of FRET was observed from lower acceptor concentration of 5 mole% (Figure 21).

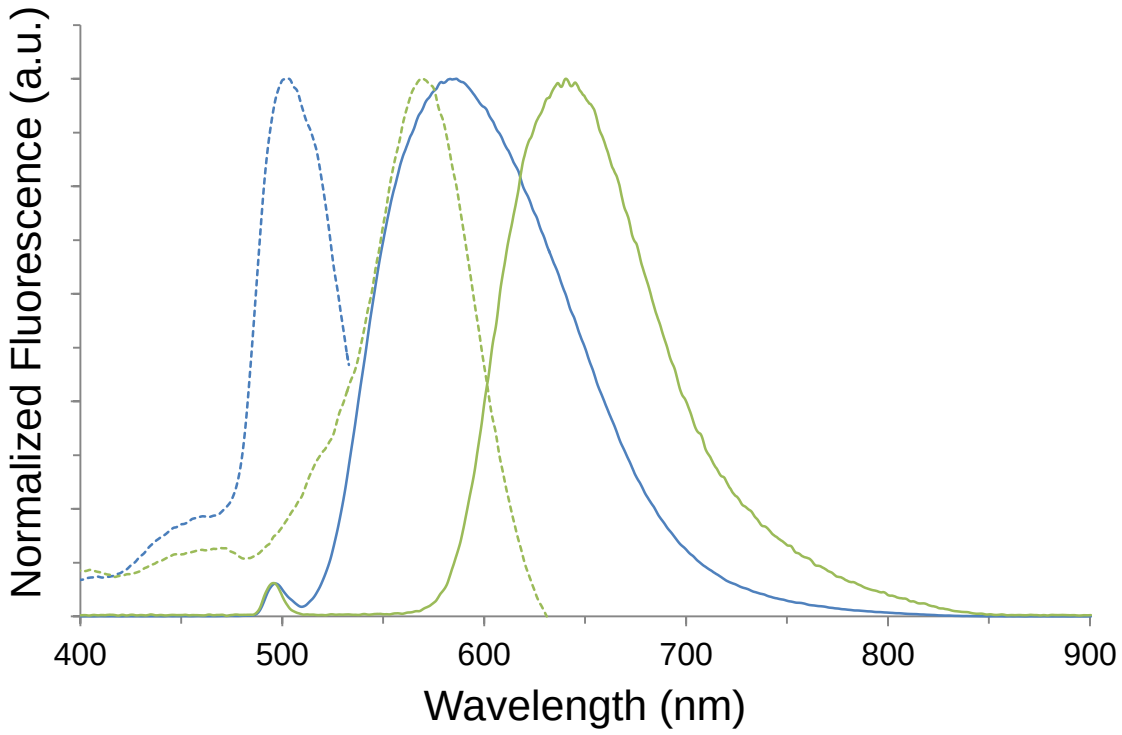

Figure 20. Fluorescence emission (solid line, excited at 500nm) and excitation (dotted line, monitored at λ_{em}) spectra of 5mM **BTD-P** TCE gel (blue) and 5mM **BTD-P** TCE gel with 10mole% **NDI-P-2** (green).

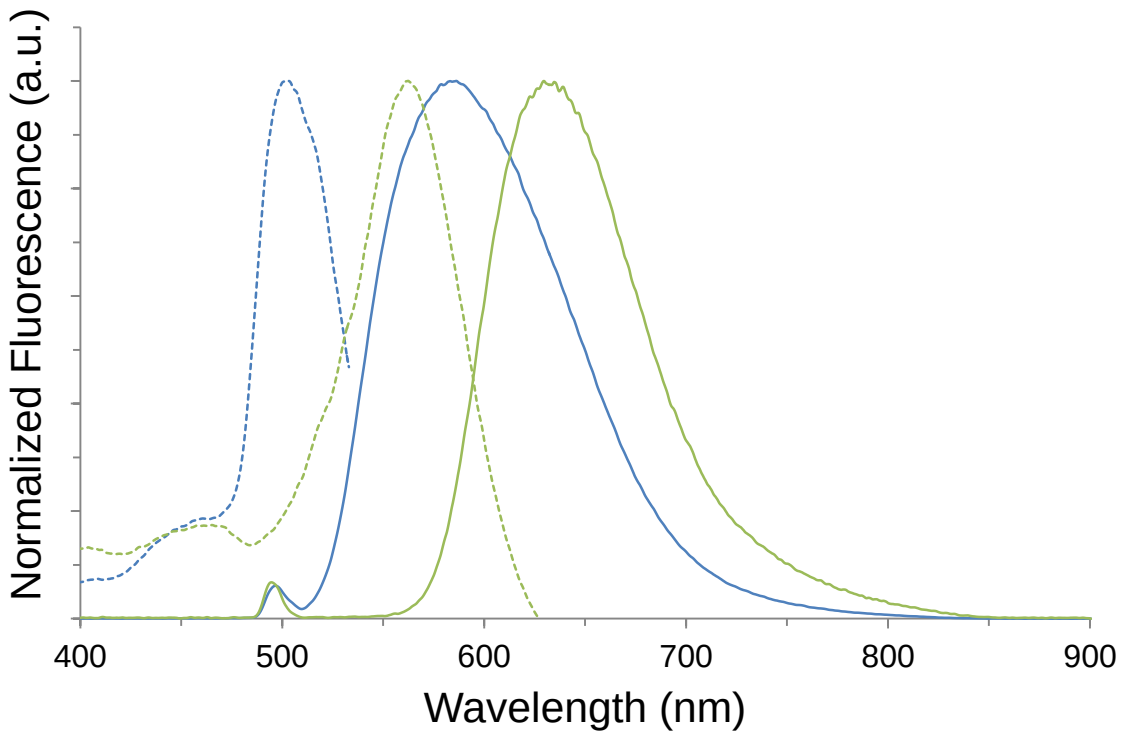

Figure 21. Fluorescence emission (solid line, excited at 500nm) and excitation (dotted line, monitored at λ_{em}) spectra of 5mM **BTD-P** TCE gel (blue) and 5mM **BTD-P** TCE gel with 5mole% **NDI-P-2** (green).

To verify the emission of **BTD-P**/**NDI-P-2** at the indirect excitation is through FRET, the solution fluorescence of **NDI-P-2** at λ_{exc} = 500 nm was tested. As shown in Figure 22, only negligible emission was observed from **NDI-P-2** at the excitation at 500 nm, which confirms FRET in **BTD-P**/**NDI-P-2**.

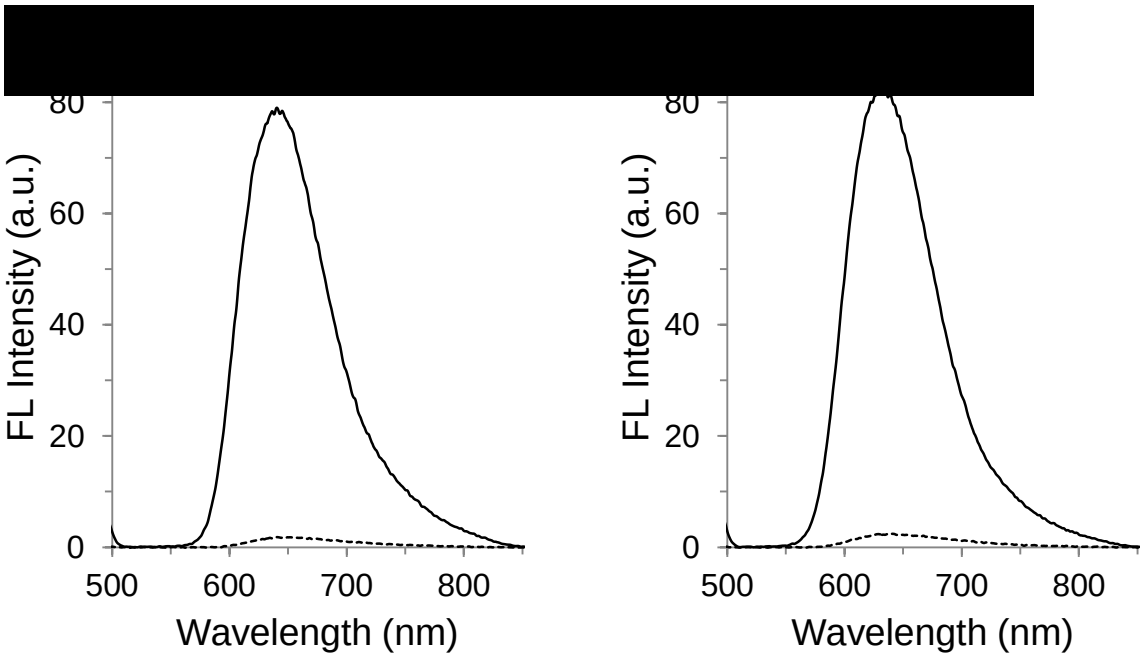

Figure 22. Fluorescence spectra (λ_{exc} = 500nm) of **A) NDI-P-2** TCE solution (0.5 mM, broken line); **BTD-P**/10mole% **NDI-P-2** TCE gel (solid line) and **B) NDI-P-2** TCE solution (0.25 mM, broken line); **BTD-P**/5mole% **NDI-P-2** TCE gel (solid line)

6 CONCLUSION

By using a strategic molecular design, four new n-type materials (**BTD-P**, **NDI-P-1**, **NDI-P-2**, **PTCDI-P**) were successfully synthesized and characterized. The molecular structures were confirmed with ^{1}H NMR, ^{13}C NMR, and high resolution mass spectroscopy analyses. Physical properties were studied thoroughly with UV-Vis and fluorescence emission spectroscopy, cyclic voltammetry, and differential scanning calorimetry. Electronic property characterization showed successful E_{LUMO} control using a molecular design with acceptor-acceptor'-acceptor (A-A'-A) configuration. By alternating A' with structural moieties of increasing electron deficiency in the order of benzothiadiazole (BTD), naphthalene diimide (NDI), and perylenetetracarboxylic diimide (PTCDI), E_{LUMO} of the whole molecules was lowered to values of -3.34 eV, -3.90, and -3.97 eV, respectively.

Through theoretical evaluation, it was found that E_{LUMO} of the title molecules is directly correlated to the electron deficiency of A'. This was seen from the calculated frontier molecular orbital diagrams which showed that LUMO is localized on A'. This confirms our molecular design is effective in tailoring electron deficiency.

All of the title molecules except for **PTCDI-P**, showed good 1D self-assembling ability. In particular, **BTD-P** gelled 1,1,1-trichloroethane. Although **NDI-P-1** and **NDI-P-2** did not form a gel, their cast films showed fibrillary morphology. In the case of **PTCDI-P**, non-flat geometry of PTCDI was revealed by theoretical evaluation which could hamper 1D self-assembly.

Charge transfer (CT) was tested using **NDI-P-1** and **NDI-P-2** with pyrene donor and characterized using UV-Vis and fluorescence spectroscopy. This revealed more efficient CT with **NDI-P-1** over **NDI-P-2**. After further analysis using polarized optical microscopy (POM), noticeable phase separation was observed for pyrene/**NDI-P-2** whereas pyrene/**NDI-P-1** showed homogeneous morphology. It was presumed that the bulky alkyl chain of **NDI-P-1** facilitates more room between molecules so that pyrene can intercalate more efficiently.

Fluorescence resonance energy transfer (FRET) through organogelation was studied with **BTD-P** as a donor and **NDI-P-2** as an acceptor. Successful gel formation and POM study confirmed 1D fibrilar structure assembly at the acceptor concentrations of 5 mole% and 10 mole%. FRET was characterized using fluorescence spectroscopy which revealed efficient FRET even at the low acceptor concentrations.

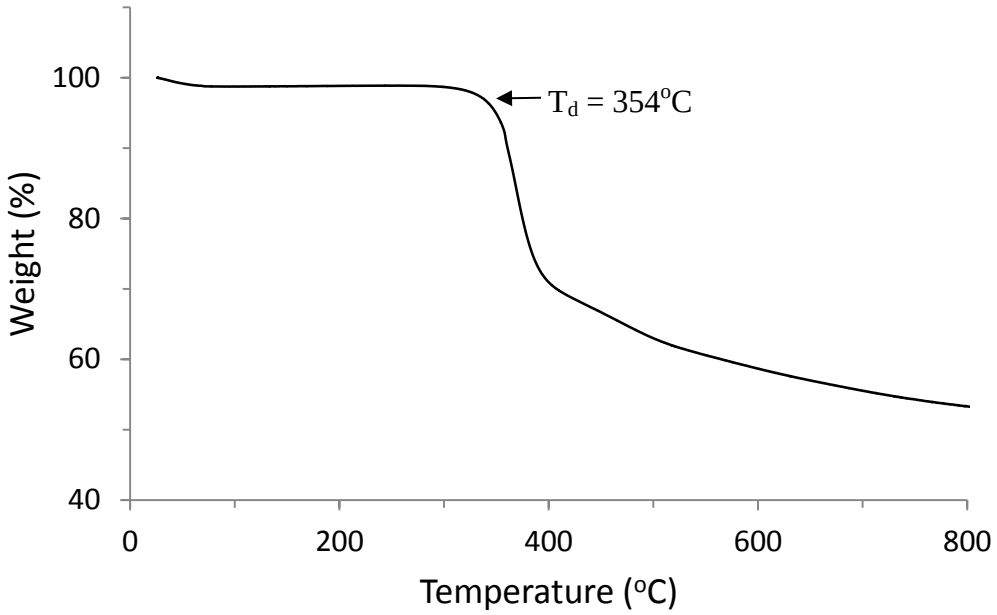

Figure S1. TGA thermogram of **BTD-P** in nitrogen at heating rate of 10°C/min.

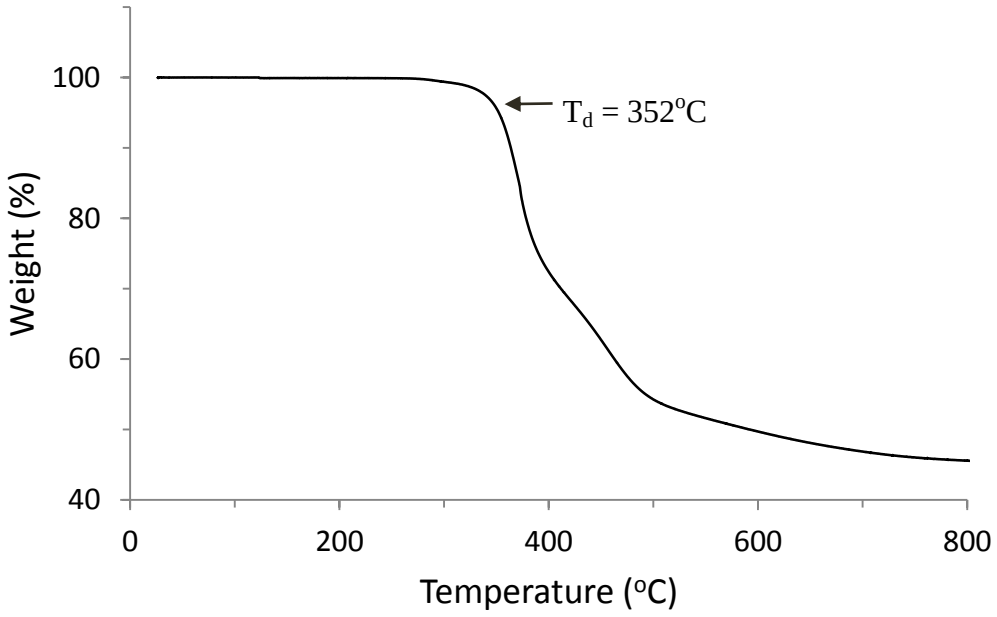

Figure S2. TGA thermogram of **NDI-P-1** in nitrogen at heating rate of 10°C/min.

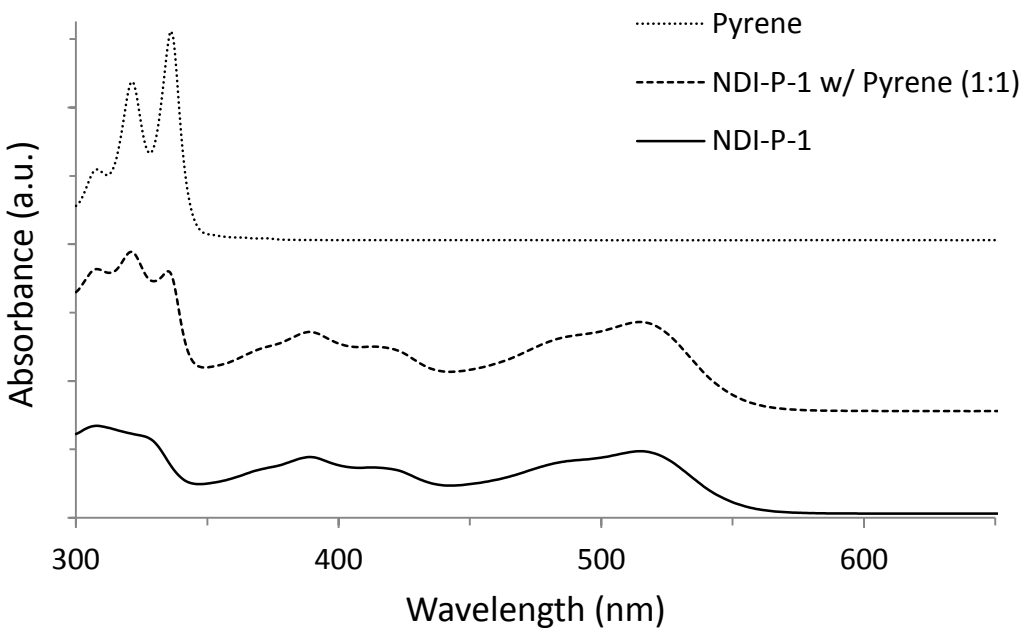

Figure S3. UV-Vis absorption spectra of **NDI-P-1, NDI-P-1** with pyrene at equal concentration, and pyrene in dichloromethane solution.

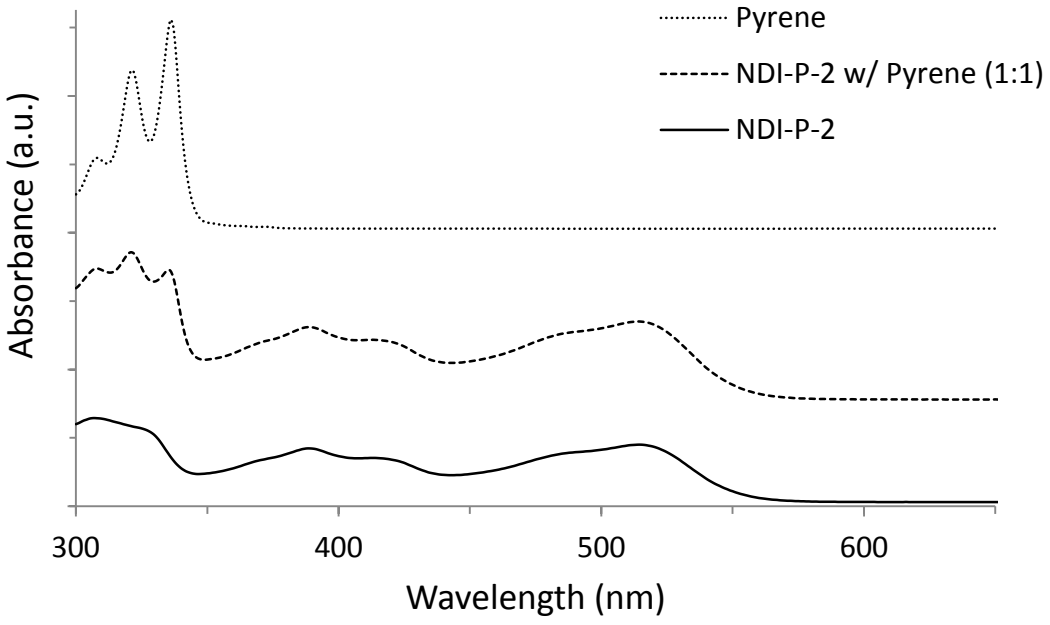

Figure S4. UV-Vis absorption spectra of **NDI-P-2**, **NDI-P-2** with pyrene at equal concentration, and pyrene in dichloromethane solution.

REFERENCES

1. Briseno, A. L.; Mannsfeld, S. C. B.; Reese, C.; Hancock, J. M.; Xiong, Y.; Jenekhe, S. A.; Bao, Z.; Xia, Y., "Perylenediimide nanowired and their use in fabricating field-effect transistors and complementary inverters" *Nano Lett.*, **2007**, *7*, 2847-2853.
2. Hansel, H.; Zettl, H.; Krausch, G.; Kisselev, R.; Thelakkat, R.; Thelakkat, M.; Schmidt, H. W. "Optical and electronic contributions in double-heterojunction organic thin-film solar cells." *Adv. Mater.*, **2003**, *15*, 2056-2060.
3. Yu, G.; Gao, J.; Hummelen, J. C.; Wudl, F.; Heegar, A. J. "Polymer photovoltaic cells: enhanced efficiencies via a network of internal donor-acceptor heterojunctions" *Science*, **1995**, *270*, 1789-1791.
4. Peumans, P.; Uchida, S.; Forrest, S. R. "Efficient bulk heterojunction photovoltaic cells using small-molecular weight organic thin films" *Nature*, **2003**, *425*, 158-162.
5. Yang, X.; Loos, J.; Veenstra, S. C.; Verhees, W. J. H.; Wienk, M. M.; Kroon, J. M.; Michels, M. A. J.; Janssen, R. A. J. "Nanoscale morphology of high-performance polymer solar cells" *Nano. Lett.*, **2005**, *5*, 579-583.
6. Lobert, M.; Mishra, A.; Uhrich, C.; Pfeiffer, M.; Bauerle, P., "Synthesis and characterization of benzo- and naphto{2,1-b:3,4-b']dithiophene-containing oligomers for photovoltaic applications" *J. Mater. Chem. C.*, **2014**, *2*, 4879-4892.
7. Chen, L. C.; Chem, J. C.; Chen, C. C.; We, C. G., "Fabrication and Properties of High-Efficiency Perovskite/PCMB Organic Solar Cells" *Nanoscale Research Letters*, **2015**, *10*, 1-5.

8. Griffith, O. L.; Liu, X.; Amonoo, J. A.; Djurovich, P. I.; Thompson, M. E.; Green, P. F.; Forrest, S. R., "Charge transport and excitation dissociation in organic solar cells consisting of dipolar donors mixed with C70" *Phys. Rev. B.*, **2015**, *92*, 85404-85409.
9. Sabirov, D. S.; Terentyev, A. O.; Cataldo, F., "Bisadducts of the C60 and C70 fullerenes with anthracene: Isomerisn and DFT estimation of stability and polarizability" *Computational & Theoretical Chemistry*, **2016**, *1081*, 44-48.
10. Nakanishi, R.; Nogimura, A.; Eguchi, R.; Kanai, K., "Electronic structure of fullerene derivatives in organic photovoltaics" *Organic Electronics*, **2014**, *15*, 2912-2921.
11. Briseno, A. L.; Mannsfeld, S. C. B.; Lu, X.; Xiong, Y.; Jenekhe, S. A.; Bao, Z.; Xia, Y., "Fabrication of field-effect transistors from hexathiapentacene single-crystal nanowires"*Nano Lett.*, **2007**, *7*, 668-675.
12. Briseno, A. L.; Mannsfels, S. C. B.; Shamberger, P. J.; Ohuchi, F. S.; Bao, Z.; Jenekhe, S. A.; Xia, Y., "Self-assembly, Molecular Packing, and Electron Transport in n-type polymer semiconductor Nanobelts" *Chem. Mater.*, **2008**, *20*, 4712-4719.
13. Schenning, A. P. H. J.; Meijer, E. W. "Supramolecular electronics; nanowires from self-asssembled π-conjugated systems" *Chem. Commun.*, **2005**, 3245-3258.
14. Murphy, A. R.; Frechet, J. M. J., "Organic semiconducting oligomers for use in thin film transistors" *Chem. Res.*, **2007**, *107*, 1066-1096.
15. Jalani, K.; Kumar, M.; George, S. J., "Mixed donor-acceptor charge-transfer stacks formed via hierarchical self-assembly of a non-covalent amphiphilic foldamer" *Chem. Commun.*, **2013**, *49*, 5174-5176

16. Hoeben, F. J. M.; Jonkheijm, P.; Meijer, E. W.; Schenning, P. H. J., "About Supramolecular Assemblies of π-Conjugated Systems" *Chem. Rev.*, **2005**, *105*, 1491-1546.
17. Zhou, E.; Tajima, K.; Yang, C.; Hashimoto, K., "Band gap and molecular energy level control of perylene diimide-based donor-acceptor copolymers for all-polymer solar cells" *J. Mater. Chem.* **2010**, *20*, 2362-2368.
18. Kulkarni, A. P.; Tonzola, C. J.; Babel, A.; Jenekhe, S. A, "Electron Transport Materials for Organic Light-Emitting Diodes" *Chem. Mater.* **2004**, *16*, 4556-4573.
19. Tonzola, C. J.; Alam, M. M.; Jenekhe, S. A., "A New Synthetic Route to Soluble Polyquinolines with Tunable Photophysical, Redox, and Electroluminescent Properties" *Macromolecules* **2005**, *38*, 9539-9547.
20. Cho, C. M.; Ye, Q.; Neo, W. T.; Lin, T.; Lu, X.; Xu, J., "Ultrahigh electron-deficient pyrrolo-acenaphtho-pyridazine-dione based donor-acceptor conjugated polymers for electrochromic applications" *Polym. Chem.* **2015**, *6*, 7570-7579.
21. Kozycz, L. M.; Guo, C.; Manion, J. G.; Tilley, A. J.; Lough, A. J.; Li, Y.; Seferos, D. S., "Enhanced electron mobility in crystalline thionated naphthalene diimides" *J. Mater. Chem. C.* **2015**, *3*, 11505-11515.
22. Zahn, D. R. T.; Kampen, T. U.; Mendez, H., "Transport gap of organic semiconductors in organic modified Schottky contacts" *Appl. Phys. Lett.* **2003**, *212*, 423-427.
23. Pandey, A. K.; Nunzi, J. M., "Upconversion injection in rebrene/perylene-diimide-heterostructure electroluminescent diodes" *Appl. Phys. Lett.* **2007**, *90*, 263508.
24. Swathi, R. S.; Sebastian, K. L., "Distance dependence of fluorescence resonance energy transfer" *J. Chem. Sci.*, **2009**, *121*, 777-787.

25. Pozzo, J. L.; Clavier, G. M.; Desvergne, J. P., "Rationel design of new acid-sensitive organogelators" *J. Mater. Chem.* **1998**, *8*, 2575-2577.
26. Fogel, Y.; Kaster, M.; Wang, Z.; Andrienko, D.; Bodwell, G. J.; Mullen, K., "Electron-Deficient N-Heteroaromatic Linkers for the Elaboration of Large, Soluble Polycyclic Aromatic Hydrocarbons and their Use in the Synthesis of Some Very Large Transition Metal Complexes" *J. Am. Chem. Soc.* **2007**, *129*, 11743-11749.
27. Kotwica, K.; Bujak, P.; Wamil, D.; Materna, M.; Skorka, L; Gunka, P. A.; Nowakowski, R.; Golec, B.; Luszczynska, B.; Zagorska, M.; Pron, A., "Indanthrone dye revisited after sixty years" *Chem. Commun.*, **2014**, *50*, 11543-11546.
28. Lee, D. C.; Jang, K.; McGrath, K. K.; Uy, R.; Robins, K. A.; Hatchett, D. W.; "Self-Assembling Asymmetric Bisphenazines with Tunable Electronic Properites" *Chem. Mater.* **2008**, *20*, 3688-3695.
29. Wurthnew, F.; Stolte, M., "Naphthalene and Perylene Diimides for Organic Transistors" *Chem. Comm.* **2011**, *47*, 5109-5115.
30. Wurthner, F, "Plastic Transistors Reach Maturity for Mass Applications in Microelectronics" *Angew. Chem. Int. Ed.* **2001**, *40*, 1037.
31. Katz, H. E. "Organic molecular solids as thin film transistor semiconductors" *J. Mater. Chem.*, **1997**, *7*, 369.
32. Zentel, R.; Jungbauer, D.; Twieg, R. J.; Yoon, D. Y.; Willson, C. G., "Synthesis and non-linear optical characteristics of crosslinked and linear epoxy polymers with pendant tolane chromophores" *Makromol. Chem.* **1993**, *194*, 859-868.
33. Li, J.; Yan, M.; Xie, Y.; Qiao, Q., "Linker effects on optoelectronic properties of alternate donor-acceptor conjugated polymers" *Energy Environ. Sci.* **2011**, *4*, 4276-4283.

34. Dincalp, H.; Murat, G.; Icli, S., "Improvement of intramolecular charge transfer within a donor-acceptor blend by doping novel synthesized benzothiadiazole small molecules in solid state" *Opt. Mater.* **2014**, *36*, 1525-1533.
35. Thalacker, C.; Röger, C.; Würthner F., "Synthesis and Optical and Redox Properties of Core-Substituted Naphthalene Diimide Dyes" *J. Org. Chem.* **2006**, *71*, 8098-8105.
36. Würthner, F.; Ahmed, S.; Thalacker, C.; Debaerdemaeker, T., "Core-Substituted Napthalene Bisimides: New Fluorophors with Tunable Emission Wavelength for FRET Studies" *Chem. Eur. J.* **2002**, *8*, 4742-4750.
37. Menacher, F.; Wagenknecht, H. A., "Synthesis of DNA with Green Perylene Bisimides as DNA Base Substitutions" *Eur. J. Org. Chem.* **2011**, 4564-4570.
38. Zhou, E.; Tajima, K.; Yang, C.; Hashimoto, K., "Band gap and molecular energy level control of perylene diimide-based donor-acceptor copolymers for all-polymer solar cells" *J. Mater. Chem.* **2010**, *20*, 2362-2368.
39. Eldridge, J. E.; Ferry, J. D., "Studies of the Cross-linking Process in Gelation Gels. III. Dependence of Melting Point on Concentration and Molecular Weight" *J. Phys. Chem.*, **1954**, *58*, 992-995.
40. Kapil, R. S, "Nitration of m-Iodonitrobenzene" *J. Chem. Soc.*, **1959**, *8*, 4127-4128.
41. Lee, D. C.; Cao, B.; Jang, K.; Forster, P. M., "Self-assembly of halogen substituted phenazines" *J. Mater. Chem.*, **2010**, *20*, 867-873.
42. Hendsbee, A. D.; Sun, J. P.; Rutledge, L. R.; Hill, I. G.; Welch, G. C., "Electron deficient diketopyrrole dyes for organic electronics: synthesis by direct arylation, optoelectronic characterization, and charge carrier mobility" *J. Mater. Chem. A.*, **2014**, *2*, 4198-4207.

43. Ajayaghosh, A.; Vijayakumar, C.; Varghese, R.; George, S. J., "Cholesterol-Aided Supramolecular Control over Chromophore Packing: Twisted and Coiled Helices with Distinct Optical, Chiroptical, and Morphological Features" *Angew. Chem. Int. Ed.*, **2006**, *45*, 456-460.
44. Kim, H.; Li, X.; Son, Y. A., "Electrochemical Study on Energy Potential Levels with Pyrene Molecule" *Textile Coloration and Finishing* **2013**, *25*, 159-164.
45. Pommerehne, J.; Vestweber, H.; Guss, W.; Mahrt, R. F.; Bassler, H.; Porsch, M.; Daub, J., "Efficient Two Layer LEDs on a Polymer Blend Basis" *Adv. Mater.* **1995**, *7*, 551-554.
46. Fukude, Y.; Shiragami, H.; Utimoto, K.; Nozaki, H., "Synthesis of Substituted Furans by Palladium Catalyzed Cyclization of Acetylenic Ketones" *J. Org. Chem.* **1991**, *56*, 5816-5819.
47. Kiitiro, U., "Palladium Catalyzed Synthesis of Heterocycles" *Pure & Appl. Chem.* **1983**, *55*, 1845-1852.
48. Chen L.; Li C.; Mullen K., "Beyond perylene diimides: synthesis, assembly and function of higher rylene chromophores" *J. Mater. Chem. C.*, **2014**, *2*, 1938-1956.
49. Goetz, K. P.; Vermeulen, D.; Payne, M. E.; Kloc, C.; McNeil, L. E.; Jurchescu, O. D., "Charge-transfer complexes: new perspectives on an old class of compounds" *J. Mater. Chem. C.*, **2014**, *2*, 3065-3076.
50. Park, S. K.; Cho, I.; Gierschner, J.; Kim, J. H.; Kim, J. H.; Kwon, J. E.; Kwon, K. O.; Whang, D. R.; Park, J. H.; An, B. K.; Park, S. Y., "Stimuli-Responsive Reversible Fluorescence Switching in Crystalline Donor-Acceptor Mixture Film: Mixed Stack Charge-Transfer Emission versus Segregated Stake Monomer Emission" *Angew. Chem. Int. Ed.*, **2016**, *55*, 203-207.

51. Zophel, L.; Enkelmann, V.; Mullen, K., "Tuning the HOMO-LUMO Gap of Pyrene Effectively via Donor-Acceptor Substitution: Positions 4,5 Versus 9,10" *Org. Lett.* **2013**, *15*, 804-807.

52. Mulliken. R. S., "Molecular Compounds and their Spectra" *J. Am. Chem. Soc.*, **1952**, *74*, 811-824.

53. Kuroda, H.; Amano, T.; Ikemoto, I.; Akamatu, H., "Charge-Transfer Interaction in Tetracyanoethylene Complexes of Pyrene and Naphthalene" *J. Am. Chem. Soc.* **1967**, *89*, 6056-6063.

54. Dandapat, M.; Mandal, D., "Fluorescence resonance energy transfer in AOT/4-chlorophenol/m-xylene organogels" *Journal of Luminescence*, **2015**, *162*, 108-114.

55. Basak, D.; Das, A.; Ghosh, S., "Hydrogen-bonding driven luminescent assembly and efficient Forster Resonance Energy Transfer (FRET) in a dialkoxynaphthalene-based organogel" *RSC Adv.*, **2014**, *4*, 43564-43571.

56. Terech, P.; Weiss, R. G., "Low Molecular Mass Gelators of Organic Liquids and their Properties as Gels" *Chem. Rev.*, **1997**, *97*, 3133-3159.

57. Ajayaghosh, A.; Praveen, V., "π-Organogels of Self-Assembled *p*-Phenylenevinylenes: Soft Materials with Distinct Size, Shape, and Functions" *Acc. Chem. Res.*, **2007**, *40*, 644-656.

58. Sangeetha, N. M.; Maitra, U., "Supramolecular gels: Functions and uses" Chem. Soc. Rev., 2005, 34, 821-836.

59. Duncan, D. C.; Whitten, D. G., "H NMR Investigation of the Composition, Structure, and Dynamics of Cholesterol-Stilbene Tethered Dyad Organogels" *Langmuir* **2000**, *16*, 6445-6452.

60. Kawano, S. I.; Fujita, N.; Van Bommel, K. J. C.; Shinkai, S., “Pyridine-containing Cholesterols as Versatile Gelators of Organic Solvents and the Subtle Influence of Ag(I) on the Gel Stability” Chem. Lett. 2003, 32, 12-13.

CURRICULUM VITAE

Graduate College
University of Nevada, Las Vegas

Kelly N. Zaugg

Degrees:

Bachelor of Science in Chemistry, 2012
University of Minnesota
Minneapolis, MN 55455

Thesis Title:

Strategic Molecular Design to Engineer the Electron Affinity of Self-Assembling Organic Semiconductors

Thesis Examination Committee:

Chairperson, Dong-Chan Lee, Ph.D.
Committee Member, Kathleen A. Robins, Ph.D.
Committee Member, Gary Kleiger, Ph.D.
Graduate Faculty Representative, Woosoon Yim, Ph.D.